# Peatland-VU-NUCOM (PVN 1.0): Using dynamic PFTs to model peatland vegetation, CH4 and CO2 emissions

Tanya J.R. Lippmann[1], Ype van der Velde[1], Monique M.P.D. Heijmans[2], Han Dolman[3,4], Dimmie M.D. Hendriks[5], and Ko van Huissteden[1,6]

[1]Vrije Universiteit, Amsterdam, the Netherlands
[2]Wageningen University and Research, Wageningen, the Netherlands
[3]Royal Netherlands Institute for Sea Research, Texel, the Netherlands
[4]Netherlands Earth System Science Center, Utrecht, the Netherlands
[5]Deltares Research Institute, Utrecht, the Netherlands
[6]VOF Kytalyk Carbon Cycle Research, Epse, the Netherlands

**Correspondence:** Tanya J.R. Lippmann (t.j.r.lippmann@vu.nl)

**Abstract.** Despite covering only 3% of the planet's land surface, peatlands store 30% of the planet's terrestrial carbon. The potential to both emit and ~~drawdown~~ take-up $CO_2$ and $CH_4$, means that peatlands have a complex and multifaceted relationship with the global climate system. The net ~~GHG~~ greenhouse gas (GHG) emissions from peatlands depends on many factors but primarily vegetation composition, ~~ground~~ water level and drainage, land management, and soil temperature. Many peatland models use ~~surface~~ water levels to estimate $CH_4$ exchange, neglecting to consider the ~~efficiency~~ role of $CH_4$ transported to the atmosphere by vegetation.

To assess the impact of vegetation on the GHG fluxes of peatlands, we have developed a new model, Peatland-VU-NUCOM (PVN). The new PVN model has been built from two parent models, the Peatland-VU and NUCOM-BOG models. The PVN model is a site-specific peatland $CH_4$ and $CO_2$ emissions model, able to reproduce vegetation dynamics. To represent dynamic vegetation, we have introduced plant functional types and competition, adapted from the NUCOM-BOG model, into the Peatland-VU model, a peatland GHG emissions model. The new PVN model includes plant competition, $CH_4$ diffusion, ebullition, root, shoot, litter, exudate production, below-ground decomposition, and above-ground moss development, under changing water levels and climatic conditions.

Here, we present the PVN model structure and explore the model's sensitivity to environmental input data and the introduction of the new vegetation-competition schemes. We evaluate the model against observed chamber data collected at two peatland sites in the Netherlands to show that the model is able to reproduce realistic plant biomass fractions, and daily $CH_4$ and $CO_2$ fluxes. We find that this process based model is suitable to be used to simulate peatland vegetation dynamics, $CH_4$ and $CO_2$ emissions.

## 1 Introduction

~~Peatlands are the world's largest terrestrial carbon store.~~ Despite covering only 3% of the planet's land surface, peatlands store 30% (644 GtC) of the planet's terrestrial carbon (Yu et al., 2010)~~, equivalent to 60% of the atmospheric carbon pool~~. The

present day global radiative effect of peatlands on the climate ~~are~~ is estimated to be between -0.2 and -0.5 $\mathrm{Wm}^{-2}$ (i.e. a net cooling) (Frolking and Roulet, 2007), in comparison to a radiative forcing of +2.43 $\mathrm{Wm}^{-2}$ due to all anthropogenic greenhouse gases since pre-industrial times (**?**). Future changes to the climate will impact the carbon sequestration capacity of peatlands, however, the net effect of climate change on peatlands is not yet understood (Loisel et al., 2021). Research indicates that some peatlands will form a positive feedback (Dorrepaal et al., 2009)~~, ~~; whist others will form a neutral (Saleska et al., 2002), or negative feedback to warming of the global climate system (Melillo et al., 2002; Lafleur et al., 2003) and the net effect of these complex responses is not yet known.

The net warming effect of peatlands on the global climate system, and particularly whether peatlands function as a carbon source or sink, is dependent on the net ~~emission~~ emissions of two of the most ~~prevelant~~ prevalent atmospheric greenhouse gases, $CO_2$ and $CH_4$. Peatlands are large natural sources of global atmospheric $CH_4$ (Spahni et al., 2011). Between 2005 and 2008~~(Doblas-Reyes et al., 2021)~~, natural $CH_4$ emissions (e.g. peatlands, lakes, other wetlands etc.) contributed approximately 50% of total $CH_4$ emissions (Saunois et al., 2020). Natural $CH_4$ emissions, particularly from wetlands, are ~~the greatest~~ a great source of uncertainty in the global methane budget (Saunois et al., 2020). There exists a need to better constrain this estimate, requiring a better understanding of small scale processes (Bridgham et al., 2013). In peatlands, $CH_4$ is produced by anaerobic microbial communities found in the soil layer and therefore, the water level height plays a critical role on the net $CH_4$ flux (Bridgham et al., 2013).

The potential to both emit and drawdown $CO_2$ and $CH_4$, means that peatlands have a complex and multifaceted relationship with the global climate system. The net ~~GHG~~ greenhouse gas (GHG) emissions from peatlands depends on many factors but primarily vegetation composition, land management, ground water level and drainage, and soil temperature (Dorrepaal et al., 2009; **?**). Rewetting drained peatlands is one strategy proposed to combat enhanced $CO_2$ emissions from peatlands but has been documented to both enhance and reduce GHG emissions (eg. Günther et al. (2020); **?**) with the majority of studies concluding that rewetting leads to enhanced $CH_4$ and net GHG emissions, sometimes persisting for decades (Harpenslager et al., 2015; Knox et al., 2015). Rewetting refers to the practice of re-raising surface water levels of drained peatlands (Knox et al., 2015). Field studies have shown that vegetation restoration in combination with rewetting may reduce GHG emissions (**???**). Vegetation impacts the net GHG emissions in peatlands by directly influencing the net primary production ~~(photosynthesis minus plant respiration)~~ and organic matter available for decomposition and indirectly, by influencing the substrates available for microbial metabolization in the soil column. *Sphagnum* is a primary contributor to the carbon sequestration in ~~peatlands and decompose~~ many peatlands and decomposes three times slower than most vascular plants (**?**). Spatial variation in the rate of vegetation growth and decomposition, particularly for bryophyte species, leads to the creation of microforms, such as hummocks, hollows and lawns which in turn impact the water level relative to the surface and spatially variable fluxes (**?**). To understand the role of vegetation emissions' feedbacks during peatland restoration efforts, vegetation must thus be treated as a dynamic interactive element of the peatland ecosystem.

~~There is an urgent need to expand model development efforts to assess the role of vegetation on GHG emissions of peatlands, particularly for peatland restoration efforts. Many peatland carbon cycle models have been developed over the preceding decades and~~ While the effects of groundwater table on peatland GHG emissions are extensively described (**?**), the ~~Wetland~~

and Wetland impacts of plant type and plant community composition on GHG emissions are less understood (**?**). Differences in vegetation composition within the same site and with the same water levels have been observed to lead to differences in $CH_4$ Inter-comparison of Models Project (WETCHIMP) evaluated the ability of a variety of models to simulate large-scale wetland characteristics and corresponding emissions (Melton et al., 2013; Wania et al., 2013). WETCHIMP showed that peatland modelling efforts have made significant advancements to simulate fluxes by including specific processes such as plant transport and ebulition. However, many models still use fluxes (**??**). Plant functional types have been found to explain uncertainties in GHG emissions from wetlands in response to warming in a meta-analysis of wetlands exposed to warming (**?**). Changes in vegetation composition have been observed in long running water table manipulation experiments (**??**). Generally, sedges and mosses establish during wetter conditions and shrubs and trees develop during dryer conditions, with enhanced *Sphagnum* growth out-competing shrubs during warming experiments (Dorrepaal et al., 2006). Below-ground, changes in vegetation have been accompanied by changes in bacterial and fungal biomass (**?**) as well as changes in methanogenic and methanotrophic community diversity (**??**). Following changes in plant community composition, changes to $CO_2$ and surface water levels as indicators of exchange (Metzger et al., 2015). There exist only two pre-existing models that simulate peatlands, dynamic vegetation and (NPP) have been observed, further impacting root exudation (**?**). Root exudates are a diverse group of organic compounds secreted by plant roots into the nearby soil. The composition and quality of root exudates varies between plant types, leading to the attraction of particular microorganisms, influencing community composition and function, $CO_2$ & (**?**) and $CH_4$ cycling (i. e. PEATBOG (Wu et al., 2016) and LPJ-WHyMe (Wania et al., 2010)) thereby limiting the ability to assess model mechanistic processes. The functionality and scope of current models that simulate peatlands and include either dynamic or static vegetation are compared in Table fluxes (**?**). Peat mineralization rates were observed to decline as readily decomposable material is already mineralized (**?**Dorrepaal et al., 2009). Plant growth, root exudation and decomposition of organic matter happen at rates that differ depending on plant type (Dorrepaal et al., 2007).

Plants with common ecosystem functions or structures (Wullschleger et al., 2014) can be represented with common model algorithms or parameters in a vegetation model when grouped as Plant Functional Types (PFTs) (Wullschleger et al., 2014). Shifts in community composition lead to feedbacks between species and other environmental parameters such as soil moisture, bulk density, soil organic matter (SOM) content, gas conduit function, rate of growth, rate of decomposition, microbial mineralisation, aerobic decomposition (De Boeck et al., 2011). Dynamic (rather than static) PFTs simulate the inter-seasonal growing and dying of plants, that over a number of years lead to vegetation succession, and are critical to reliably assess the impacts of climate and environmental change on peatland ecosystems (Box et al., 2019). Plant growth, root exudation and decomposition of organic matter happen at rates that differ depending on the plant type (Dorrepaal et al., 2007). Ecosystem storage of carbon happens through uptake by photosynthesis and the slow decomposition of plant matter, leaf and root detritus, and root exudates in the anaerobic zone, but the efficiency of these processes vary between species. Plant detritus and root exudate excretion play a critical role in the availability of carbonic compounds and these vary depending on plant type. It has been shown that dynamic plant representation is critical to reliably simulate vegetation-environmental feedbacks in models (Toet et al., 2006) and therefore, the inclusion of dynamic vegetation classes is critical to reliably estimate C, $CO_2$ and $CH_4$ emissions from peatlands during periods of environmental change (Li et al., 2016; **?**).

Many peatland carbon cycle models have been developed over the preceding decades. The Wetland and Wetland $CH_4$ Inter-comparison of Models Project (WETCHIMP) evaluated the ability of a variety of models to simulate large-scale wetland characteristics and corresponding $CH_4$ emissions (Melton et al., 2013; Wania et al., 2013). Peatland modelling efforts have made significant advancements to simulate $CH_4$ fluxes by including $CH_4$ specific processes such as $CH_4$ plant transport and ebullition. However, many models rely on $CO_2$ fluxes or surface water levels as indicators of $CH_4$ exchange (Metzger et al., 2015), restricting their capacity to assess feedbacks between environmental change and the peatland $CH_4$ cycle. There exist only two pre-existing models that simulate dynamic vegetation, $CO_2$, and $CH_4$ cycling in peatlands (i.e. PEATBOG (Wu et al., 2016) and LPJ-WHyMe (Wania et al., 2010)) thereby, limiting the ability to assess model mechanistic processes. The functionality and scope of current models that simulate peatlands and include either dynamic or static vegetation are compared in Table S1.

To assess the impact of dynamic vegetation classes on subsequent GHG fluxes in peatlands we ~~develop~~ present a new model, Peatland-VU-NUCOM v1.0 (PVN). PVN incorporates features of NUCOM-BOG, ~~an ecosystem competition plot-scale~~ a plot-scale ecosystem competition model (Heijmans and Berendse, 2008) into the Peatland-VU model framework, a ~~peatland~~ process-based plot-scale peatland model (van Huissteden et al., 2006). The NUCOM-BOG model simulates vegetation competition, C, nutrient, and water cycling in undisturbed bog ecosystems under changing climates~~. The NUCOM-BOG model simulates~~ , using a soil profile divided by ~~the~~ an acrotelm-catotelm boundary where plant growth and decomposition ~~is~~ are partitioned between plant organs. The Peatland-VU model simulates the $CH_4$ and $CO_2$ cycle within a column of peat soil with varying water ~~level~~levels. The Peatland-VU model simulates $CH_4$ fluxes, gross primary productivity and $CO_2$ cycle whilst assuming a constant plant layer and does not include a nitrogen cycle. ~~We evaluate the new PVN model using automated flux-chamber observations measured at two rewetted previously drained peatland sites in the Netherlands.~~ The inclusion of dynamic vegetation classes into the PVN model provides a model that is capable of ~~investigating the impact of plant restoration efforts on GHG emissions from peatlands. All three models (NUCOM, PeatlandVU, and PVN) depend heavily on calibration using (often limited) observational data and for this reason, we do not expect to reproduce observed~~ estimating the greenhouse gas balance in response to environmental changes (changes in temperature or radiation or water levels) and ~~more accurately. However, the aim is to create a model that reproduces the effects of plant species composition, changes thereof over time, and land management on GHG emissions.~~ also different management efforts (changes in harvest regime or vegetation restoration) for peatland sites. Therefore, the model can serve wetland management by estimating changes in the greenhouse gas balance of peatland sites in response to management decisions, whilst considering effects of environmental change.

## 2 Materials and Methods

~~The PVN model describes the vegetation , C, water, and dynamics of a column of an above- and below-ground peatland ecosystem. This new model incorporates key features of the NUCOM-BOG model (Heijmans and Berendse, 2008) on plant specific traits and plant competition of peatland ecosystems systems into the framework of the Peatland-VU model (van Huissteden et al., 20 The key strengths of the Peatland-VU model are to simulate and emissions, and the decomposition and production of below-ground SOM pools. The and pools and processes of the new PVN model are shown in the model schematic in . Extensive descriptions of~~

the original NUCOM and Peatland-VU models can be found in Heijmans and Berendse (2008) and van Huissteden et al. (2006); **?**, respectively.

### 2.1 Model overview

With the aim of developing a peatland model capable of reproducing the impacts dynamic PFTs have on and emissions in peatlands, the new PVN model incorporate features of the NUCOM-BOG model Heijmans and Berendse (2008) into the framework of the Peatland-VU model van Huissteden et al. (2006); **?**.

### 2.1 The PVN model

The new PVN model describes the vegetation, $CH_4$ and $CO_2$ dynamics of a column of an above- and below-ground peatland ecosystem (Fig. 1). Carbon dioxide and $CH_4$ emissions enter the atmosphere by ebullition, transport through plants, diffusion through the soil, and respiration. The PVN model computes and simulates processes on a daily time step, as does the Peatland-VU model. Prior to this version of the model, the Peatland-VU model simulations were up to seven years in duration (**?**). The NUCOM-BOG model simulates vegetation succession and carbon balance over multi centennial timescales. We compare the new PVN model against the Peatland-VU model using multi decadal model simulation results. The Peatland-VU model is driven by daily air temperature ($T$), water level (WL), radiation, a soil parameter input file, and a general model parameter input file. The new PVN model has the same input requirements as the Peatland-VU model but now also requires input parameters for each PFT, discussed in **??** and 2.3above-ground carbon pools are above-ground living biomass, litter layer (non-moss PFTs only), shoots, and living moss depth (moss PFTs only). The below-ground carbon pools are peat, labile organic matter, microbial biomass, litter & dead roots, and root exudates (Table S2).

### 2.2 Dynamic Plant Functional Types

Plant Functional Types (PFT) are the key element of NUCOM that is added to the Peatland-VU framework to create the PVN model. Any number of PFTs can be included in the a model simulation. In this study we limit our simulations to six PFTs (*Typha*, sedges, tall grasses, short grasses, *Sphagnum*, and brown mosses) based on the vegetation communities observed at our test sites. Extensive descriptions of these PFTs are described in 2.3. PFT attributes (parameters) describe plant physiology , plant dynamics or and bioclimatic limits. Each PFT has prescribed favourable temperatures and water levels for growth Bioclimatic limits are used by the photosynthesis function (Sect. 2.1.1), and the potential growth function (Eq. 13). Each PFT is defined as being either a moss or vascular plant type which, impacts the ability of plants to grow vertically or develop roots. Each PFT is prescribed as having either evergreen or deciduous phenology. For deciduous vegetation, leaf senescence biomass is adjusted to represent the leaf senescence that occurs when daily temperatures fall below minimum tolerated temperatures . (Eq. 2.1.4). For evergreen vegetation, biomass is adjusted to represent the death of old leaves (Eq. 9). Maximum leaf coverage is maintained as long as daily water level and temperature are within the ideal thresholdrange. The PFT parameters are defined in Table 1 and the values and references are listed in Table **??** and Table S3, respectively. Model processes calculated per PFT

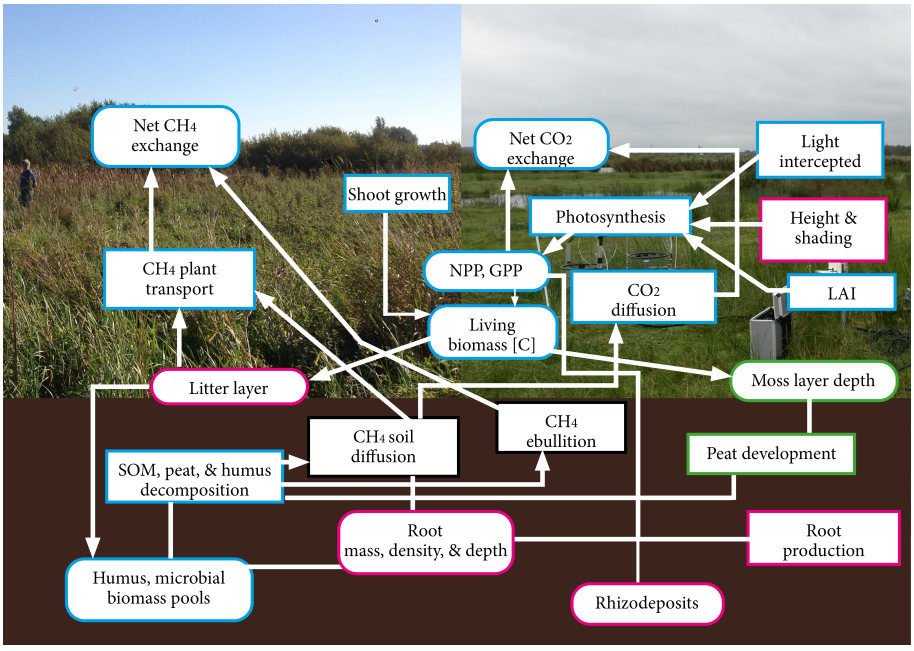


**Figure 1.** Schematic of the ~~production, consumption and~~ movement of transport of carbon in the model. ~~Dynamics and processes~~ Processes are delineated with rectangles, whereas carbon pools are delineated with curved edges. The pink outline represents non-moss pools and processes, green outline represents pools and processes and processes applicable only to moss PFTs and the blue outline refers to pools and processes that are applicable for all plant types. In the background of this figure, the Horstermeer site is shown on the left and the Ilperveld on the right.

~~are represented using a '~~In this section, the subscript, $p$~~' in the model equations.~~, is used to show that the equation or variable is PFT specific, $z$ to indicate that the equation or variable is soil layer specific, $t$ to represent time, $T$ represents temperature, and $WL$ represents water level. The convention used in this manuscript is that a positive flux represents the movement of gas from the ecosystem to the atmosphere.

~~List and description of the PFT input parameters. The values assigned to each PFT are listed in Table ??. Associated references are listed in Table S3. In the left column each PFT parameter is tied to its relevant model mechanism. Note that some PFT parameters are, at times, used by multiple model processes. Corresponding model process Parameter Description BiomassSenescence Fraction of above-ground biomass littered each day AutumnLitter For deciduous plants, fraction of leafy biomass littered each day during autumnCBiomassRatio C to biomass ratio ShootsFactor Mass fraction of primary production that consists of shoots; the remainder is root growth MaxCanopyHeight Maximum height PlantResp0 Plant respiration at zero degrees Temp_MaxPhoto Maximum temperature limit for photosynthesis Temp_MinPhoto Minimum temperature limit for photosynthesis TMinGrowth Minimum temperature for growth TOptMinGrowth Lowest temperature for optimal growth TOptMaxGrowth Highest temperature for optimal growth TMaxGrowth Maximum temperature for growth LeafRespirationCoeff Leaf maintenance respiration coefficient MaxGrowthRate Maximum growth rate SpecificLeafArea Ratio of leaf area to dry leaf mass MinLAI Minimum LAI MaxLAI Maximum LAI LightExtCoeff Light extinction coefficient MethanePlantOx Fraction of that is oxidized during plant transport MethanePType Vegetation type factor for gas transport through plant.MaxRootDepth~~

Maximum root depth RootSenescence Proportion of root mass that dies during each timestep ExudateFactor Mass fraction of of below-ground production that consists of exudates SpringCorrection Coefficient for stronger exudation in spring LitterConversion Conversion factor of above-ground to below-ground litter; the factor is temperature adjusted such that at 0 degrees the conversion factor is also 0 ResistFrac Fraction of decomposed organic material that is transferred to resistant humus fraction AssimDissim The amount of C from decomposed organic matter converted to microbial biomass WLMin Minimum water level for growth WLOptMin Lowest water level for optimal growth WLOptMax Highest water level for optimal growth WLMax Maximum water level for growth

### 2.1.1 PFT carbon pools and initialisationPrimary production

The C3 photosynthesis, leaf respiration ($RT$), and net primary production (NPP) are calculated using a modified version of the primary production scheme, introduced into the Peatland-VU model by **?**, modified from the BIOME3 equilibrium biosphere model **?**. The BIOME3 model is based on the premise that GPP and leaf respiration increase with the activity of (Rubisco) photosynthetic enzymes in leaf chloroplasts. Photosynthesis is calculated using stomatal conductance and Rubisco activity of leaves. The net $CO_2$ fluxes (NEE) for each PFT are the sum of gross primary production (GPP [kg C $m^{-2}$ $day^{-1}$]), plant respiration, $CO_2$ produced by below-ground carbon pools are peat, labile organic matter, exudates, microbial biomass, litter & dead roots, and root exudates. The above-ground carbon pools are living biomass, litter layer (non-moss PFTs only), shoots, and living moss depth (moss PFTs only) are initialised. The model generates a soil horizon representation using soil layers of equal thicknesses. The generated soil horizon uses properties such as DBD, SOM ratio, clay & sand content, C:N ratio specified in the soil profile. The number, depth, and thickness of the site's soil horizons can be adjusted in the soil input file. Following the developmentof the model's soil horizon, the root density, root distribution, aerobic SOM decomposition, and root mass of each PFT is mapped to the layout of the model's soil horizon representation (depth, density, layer thickness) . To account for differences in decomposition rates among roots, and exudates, each PFT has designated SOM pools, which are partitioned between the soil layers. Root distribution, $CO_2$ oxidised from $CH_4$ ($Rox$).

$$GPP_{t,p} = \frac{JE_{t,p} + JC_{t,p} - \sqrt{(JE_{t,p} + JC_{t,p})^2 - 4 \cdot JE_{t,p} \cdot JC_{t,p}}}{20 \cdot WSF_{t,p}} \quad (1)$$

where, $JE$ [kg C $m^{-2}$ $day^{-1}$] describes the relationship of photosynthesis to photosynthetically active radiation (PAR) and $JC$ [kg C $m^{-2}$ $day^{-1}$] describes the Rubisco limited rate of photosynthesis. $JE$ and root mass decrease exponentially from the surface to the PFT maximum root depth. In this section, the subscript $p$ is used to show that the equation or variable is PFT specific, $z$ to indicate that the equation or variable is soil layer specific, and $JC$ are defined by Eq. S2 and Eq. S10, respectively (**??**). Interactions among leaf area development, photosynthetic activity, stomatal conductance, temperature and water availability have been widely recognised (**??**). Water stress has a significant impact on plant photosynthetic capacity (**?**). Studies such as **??** have considered these factors when simulating GPP by introducing water use efficiency terms. Model intercomparison efforts have found improved reporducaibility of GPP estimates from models that account for the the impacts

**Table 1.** Name, units, description and values of PFT input parameters. Associated references are listed in Table S3. In the left column each PFT parameter is tied to its relevant model mechanism. Note that some PFT parameters are, at times, used by multiple model processes.

| Corresponding model process | Parameter | Units | Description | Tall grass | Sedges | *Typha* | *Sphagnum* | Brown moss | Short grass |
|---|---|---|---|---|---|---|---|---|---|
| Above-ground biomass | BS | - | Fraction of above-ground biomass converted to litter | 0.04 | 0.04 | 0.04 | 0.01 | 0.015 | 0.03 |
| | KL | - | Fraction of biomass converted to litter during autumn, for deciduous plants | 0.1 | 0.1 | 0.1 | 0.01 | 0.04 | 0.06 |
| | CBiomassRatio | - | Carbon to biomass ratio | 0.46 | 0.46 | 0.46 | 0.44 | 0.44 | 0.44 |
| | RS | - | Fraction of growth that consists of shoots. Remainder is root growth | 0.7 | 0.7 | 0.7 | 1.0 | 1.0 | 0.9 |
| | MaxCanopyHeight | m | Maximum height | 1.5813 | 2.5813 | 2.5813 | 0.1 | 0.2 | 0.4 |
| Photosynthesis & respiration | $T_{MaxPhoto}$ | °C | Maximum temperature for photosynthesis | 38 | 40 | 35 | 30.0 | 30.0 | 30 |
| | $T_{MinPhoto}$ | °C | Minimum temperature for photosynthesis | -3 | -1 | -3 | -1.0 | 0.5 | -1 |
| | $T_{min}$ | °C | Minimum temperature for growth | 7 | 2 | 2 | -1.0 | 0.5 | 0.5 |
| | $T_{minopt}$ | °C | Lowest temperature for optimal growth | 9 | 12 | 12 | 14.0 | 5.0 | 14 |
| | $T_{maxopt}$ | °C | Highest temperature for optimal growth | 20 | 30 | 30 | 25.0 | 25.0 | 25 |
| | $T_{max}$ | °C | Maximum temperature for growth | 45 | 45 | 45 | 38.0 | 38.0 | 38 |
| | Rc | - | Leaf maintenance respiration coefficient | 0.015 | 0.015 | 0.015 | 0.016 | 0.014 | 0.014 |
| | Rr | - | Leaf respiration coefficient | 0.015 | 0.015 | 0.015 | 0.016 | 0.014 | 0.014 |
| | Gmax | $gC day^{-1}$ | Maximum growth rate | 0.07 | 0.07 | 0.07 | 0.045 | 0.05 | 0.05 |
| LAI | SLA | $m^2 g^{-1}$ | Ratio of leaf area to dry leaf mass | 0.012 | 0.012 | 0.012 | 0.02 | 0.02 | 0.02 |
| | MinLAI | $m^2 m^{-2}$ | Minimum LAI | 0.1 | 0.1 | 0.1 | 0.1 | 0.1 | 0.1 |
| | MaxLAI | $m^2 m^{-2}$ | Maximum LAI | 3 | 4 | 4 | 1.2 | 1.5 | 1.5 |
| | LEC | - | Light extinction coefficient | 0.5 | 0.46 | 0.5 | 0.95 | 0.95 | 0.95 |
| $CH_4$ scheme | PlOx | - | Fraction of $CH_4$ consumed by rhizospheric oxidation | 0.4 | 0.4 | 0.25 | 0.7 | 0.8 | 0.6 |
| | vP | - | Vegetation type factor for gas transport through plants | 5 | 6 | 10 | 2.0 | 2.0 | 2 |
| Root processes | MRD | m | Maximum root depth | 0.46 | 1 | 1 | 0.1 | 0.1 | 0.2 |
| | RSX | $day^{-1}$ | Proportion of root mass that dies during each time step | 0.05 | 0.05 | 0.05 | 0.01 | 0.01 | 0.05 |
| | REX | - | Fraction of of below-ground production that consists of exudates | 0.1 | 0.2 | 0.2 | 0.0 | 0.0 | 0.11 |
| | KSP | - | Coefficient for stronger exudation in spring | 0.2 | 0.4 | 0.4 | 0.0 | 0.0 | 0.1 |
| Below-ground decomposition | LC | $day^{-1}$ | Conversion factor of above-ground to below-ground litter. 0 °C, LC is set to 0. | 0.005 | 0.001 | 0.001 | 0.01 | 0.005 | 0.003 |
| | HU | - | Fraction of decomposed organic material transferred to resistant humus fraction | 0.55 | 0.42 | 0.3 | 0.9 | 0.9 | 0.9 |
| | MI | - | The amount of carbon from decomposed organic matter converted to microbial biomass | 2.25 | 2.2 | 2.2 | 2.4 | 2.3 | 2.3 |

**Table 1.** Continued.

| Corresponding model process | Parameter | Units | Description | Tall grass | Sedges | *Typha* | *Sphagnum* | Brown moss | Short grass |
|---|---|---|---|---|---|---|---|---|---|
| Water level | $WL_{min}$ | m | Minimum water level for growth | -1 | -1 | -1 | -0.5 | -0.35 | -0.35 |
| | $WL_{minopt}$ | m | Lowest water level for optimal growth | -0.4 | -0.3 | -0.4 | -0.2 | -0.15 | -0.15 |
| | $WL_{maxopt}$ | m | Highest water level for optimal growth | -0.2 | -0.2 | 0 | -0.05 | -0.05 | -0.05 |
| | $WL_{max}$ | m | Maximum water level for growth | 0.0192 | 0.1 | 0.3 | 0.05 | 0.05 | 0.05 |

of water stress on photosynthetic capacity (**??**). GPP in the PVN model is modified by both a water stress factor (WSF, Eq. S1) and a temperature stress factor ($\phi_T$, Eq. S4, adapted from **?**).

$$NPP_{t,p} = GPP_{t,p} - \int_{z}^{0} Rd_{t,p} dz - RT_{t,p} \tag{2}$$

where, $RT$ [kg C m$^{-2}$ day$^{-1}$] represents daily leaf respiration, and $Rd$ [kg C m$^{-2}$ day$^{-1}$] represents the daily root respiration (Eq. 16).

$$RT_{t,p} = Rr_p \cdot VM_{t,p} \tag{3}$$

where, $Rr$ [-] is the ~~subscript *t* to represent time~~leaf respiration coefficient (Table 1), and $VM$ [kg C m$^{-2}$ day$^{-1}$] represents the maximum daily rate of net photosynthesis (Eq. S11, **??**). The $CO_2$ flux from each soil layer ($B_{CO_2}$) is calculated before integrating over all layers and summed with $CO_2$ produced by decomposed litter ($LLd$), and NPP is subtracted.

$$NEE_{t,p} = \int_{z}^{0} B_{CO_{2,t,p,z}} dz + LLd_{t,p} - NPP_{t,p} \tag{4}$$

where, $NEE$ [kg C m$^2$ day$^{-1}$] is the Net Ecosystem Exchange, $B_{CO_2}$ [kg C m$^{-2}$ day$^{-1}$] is the $CO_2$ flux produced by below-ground SOM decomposition (Eq. 26).

### 2.1.2 Competition among PFTs

Biomass fraction ($BF$) is a representation of the ratio of PFT biomass to total biomass (Eq. 5). The sum of all PFTs ~~are~~ is constrained to a maximum BF of 1.0. All PFTs have a minimum BF of 0.1 and are able to further establish when the conditions

become favourable, as adapted from the NUCOM-BOG model.

$$BF_{t,p} = \frac{CB_{t,p}}{\sum_{p=1}^{P}(CB_{t,p})}$$

$$BF_{t,p} = \frac{CB_{t,p}}{\sum_{p=1}^{P}(CB_{t,p})} \quad (5)$$

where, $CB$ ~~= biomass~~ [kg C m$^{-2}$] ~~, $t$ refers to time, and $p$ refers to PFT.~~

### 2.1.3 ~~Competition among PFTs~~

represents above-ground living biomass (Eq. 9). Each plant competes for light where taller PFTs have monopoly over shorter PFTs. Light that is not intercepted by the tallest PFT, becomes available to the next PFT, in descending height order. Light which is not intercepted by the ~~non-moss PFTs~~ vascular PFTs ($_v$) is passed on and divided between moss PFTs ($_{mp}$), proportional to their BF. In this way, an increase ~~(decrease)~~ of foliage of taller PFTs may reduce ~~(increase)~~ the growth rates of mosses due to shading by limiting light exposure. ~~At the beginning of each model day, non-moss~~ Each time step, vascular PFTs are ordered according to descending height so that the shading by taller PFTs impacts the amount of light available to shorter PFTs. ~~Plant height m~~The height of vascular PFTs is calculated using an allometric relationship ~~adapted from Huang et al. (1992); Smith et al. (2001)~~ (Eq. 6~~and~~ ) :

$$H_{t,p} = k_1 \cdot D_{t,p}^{k_2}$$

~~where,~~ ) adapted from Huang et al. (1992); Smith et al. (2001); Krinner et al. (2005) which, relates vegetation biomass to height. This relationship, initially intended to be used for trees has since been used to calculate the heights of natural and agricultural grasses in a dynamic global vegetation model (Krinner et al., 2005). Biomass and stem density have been found to respectively explain 98% and 81% of the height variance in 65 plots of 29 different species (**?**) because most plants are understood to be constrained by 'self-thinning' under crowding in natural stands, or by a trade-off between height and foliage growth, reflecting a trade-off between structural and functional physiological development.

$$D_{t,p}H_{t,v} = k_2 \cdot \left( \frac{4 \cdot CB_{t,p}}{BD \cdot \pi \cdot k_2} \frac{4 \cdot CB_{t,v}}{BD \cdot \pi \cdot k_2} \right)^{\frac{1}{2+k_3}\frac{k_3}{2+k_3}} \quad (6)$$

where, $H$ refers to plant height [m], $BD$ represents biomass density [kg C m$^{-3}$], ~~$k_1$~~ $k_2$ [m], ~~$k_2$ ,~~ and $k_3$ [-] ~~in and~~ are constants with values ~~1,~~ 40, and 0.85, taken from Smith et al. (2001). ~~The light absorbed ($FPAR$ ,~~ [-] is the fraction of incoming PAR absorbed by vegetation (Eq. 7) ~~by each PFT~~ and is dependent on LAI and the amount of shading ~~from taller plantsand their~~

~~LAI.~~ by taller plants.

$$FPAR_{t,non-mosst,p} = (1 - e^{-LEC_p}) \cdot CB_{t,p} \cdot SLA_p{}^{(-LEC_p \cdot LAI_{t,p})} \quad (7)$$

Where, $LEC$ represents the Light Extinction Coefficient parameter [-], ~~and $SLA$ represents~~ . LAI [$m^2$ $m^{-2}$] is calculated as a function of living biomass and the Specific Leaf Area ($SLA$ [$m^2$ $kg^{-1}$ C]. ~~The growth of the~~ ).

$$LAI_{t,p} = \begin{cases} MinLAI_p, & \text{if } LAI_{t,p} < MinLAI_p \\ CB_{t,p} \cdot SLA_p, & \text{if } MinLAI_p \leq LAI_{t,p} \leq MaxLAI_p \\ MaxLAI_p, & \text{if } LAI_{t,p} > MaxLAI_p \end{cases} \quad (8)$$

where, $CB$ [kg C $m^{-2}$] represents above-ground living biomass (Eq. 9)~~is~~ , dependent on shoot growth and biomass senescence lost to the litter layer.

$$\frac{\delta}{\delta t} CB_{t,p} = SM_{t,p} - BS_{t,p} \cdot CB_{t,p} \quad (9)$$

where, ~~$CB$ represents above-ground living biomass kg C $m^{-2}$ ,~~ $SM$ represents shoot mass [kg C $m^{-2}$ $day^{-1}$], calculated using Eq. 10, and $BS_{t,p}$ represents the fraction of above-ground biomass littered each day [$day^{-1}$].

$SM_{t,p} = RS_p \cdot NPP_{t,p}$

~~where, $NPP$ represents the Net Primary Productivity~~ Biomass senescence, $BS_p$ [~~kg C $m^{-2}$~~$day^{-1}$]~~and~~ , is set to $KL_p$ [$day^{-1}$] during Autumn, for deciduous plants.

$$SM_{t,p} = RS_p \cdot NPP_{t,p} \quad (10)$$

where, $RS$ represents the ratio of shoot to root growth ~~. If the harvest scheme is activated, as prescribed in the model input files, PFTs taller than the prescribed height are harvested. The harvest height and days are optional prescribed model parameters. Living biomass decreases according to the amount of biomass harvested (or mowed), under the assumption that biomass is uniformly distributed with height. A fixed percentage of the harvested material remains uncollected in the field and is added to the litter layer. LAI $m^2$ $m^{-2}$ is calculated () as a function of living biomass, the water growth factor ($WG$) and SLA, whilst constrained by prescribed minimum and maximum LAI values.~~

$$LAI_{t,p} = \frac{CB_{t,p} \cdot SLA_p}{(LEC_p \cdot \frac{\delta}{\delta t} LAI_{t,p} + (1 - e^{-WG_{t,p}}))}$$

where $WG$ refers to the water growth function (-)(Table 1). The allocation of root and shoot growth is a fixed fraction of NPP so that the fraction of shoot and root growth sums to 1.0. Growth of individual moss PFTs ($HG$, Eq. 11) is represented in terms of fractional cover, rather than height. A moss PFT with more cover has access to more light and gains an advantage over other mosses. Moss PFTs grow develop at different rates due to differences in the range of temperatures, and water levels they can growneeded for growth. The depth (or thickness, [m]) of both individual moss PFTs (Eq. 11), and the total living moss layer (Eq. 12) are dependent on $BF$, potential growth, and dry bulk density ($DBD$, kg C $m^{-3}$).

$$HG_{t,p} = \frac{PG_{t,p} \cdot BF_{t,p}}{DBD_{t,p,z=1}}$$

The moss The thickness of the living moss layer is not yet used by the model. Future model versions will use the thickness of the moss layer to recalculate land surface height, impacting the water level relative to the surface and also soil properties (such as DBD, pH, OM content of top soil layer(s)).

$$HG_{t,mp} = \frac{PG_{t,mp} \cdot BF_{t,mp}}{DBD_{t,mp,z=1}} \tag{11}$$

where, $_{mp}$ represents moss PFTs only, $PG$ represents potential growth ($PG$ [-], Eq. 13). The moss thicknesses of individual moss PFTs are aggregated to calculate the total ecosystem moss depth ($MHG$ ): [m]):

$$MHG = \frac{SHG_{t,p}}{\sum_{p=1}^{P} BF_{t,p}} \frac{\sum_{mp=1}^{MP}(HG_{t,mp} \cdot BF_{t,mp})}{\sum_{mp=1}^{MP} BF_{t,mp}} \tag{12}$$

where,

$$SHG_{t,p} = \sum_{p=1}^{P}(HG_{t,p} \cdot BF_{t,p})$$

The Potential growth ($PG$ [-], Eq. 13) reflects the favourability of water levels or temperatures for PFT growth, calculated using the water growth, $WG$and , and temperature growth, $TG$functions impact the development of moss PFTs by impacting the potential growth, functions, respectively. Potential growth, $WG$, and $TG$ are adapted functions from Heijmans and Berendse (2008). Potential Growth ($PG$

$$PG_{t,p} = FPAR_{t,p} \cdot Gmax_p \cdot TG_{t,p} \cdot WG_{t,p} \tag{13}$$

where, $Gmax$ is the maximum growth rate [~~., ) reflects the favourability of water levels or temperatures:~~

$$PG_{t,p} = FPAR_{p,t} \cdot Gmax_p \cdot TG_{T,t,p} \cdot WG_{W,t,p}$$

kg C $m^{-2}$ $day^{-1}$]. The $WG$ and $TG$ functions (unitless) are congruent to each other~~and therefore we have only written out the WG function:~~

$$WL_{max} - WL_{maxopt}, \text{ if } WL_{maxopt} < WL < WL_{max}$$

~~where~~ , where unfavourable temperature or water levels reduce growth.

$$WG_{t,p} = \begin{cases} 0, & \text{if } WL_t < WL_{min,p} \\ \frac{WL_t - WL_{min,p}}{WL_{minopt,p} - WL_{min,p}}, & \text{if } WL_{min,p} \leq WL_t < WL_{minopt,p} \\ 1, & \text{if } WL_{minopt,p} \leq WL_t \leq WL_{maxopt,p} \\ \frac{WL_{max,p} - WL_t}{WL_{max,p} - WL_{maxopt,p}}, & \text{if } WL_{maxopt,p} < WL_t \leq WL_{max,p} \\ 0, & \text{if } WL_t > WL_{max,p} \end{cases} \quad (14)$$

where, $WL$ ~~=~~ refers to water level, $min$ ~~(~~and $max$ ~~) = minimum (maximum ) tolerated water level,~~ refer to the minimum and maximum water levels tolerated for growth, $minopt$ and $maxopt$ refer to minimum and maximum optimum water levels for growth, respectively.

$$TG_{t,p} = \begin{cases} 0, & \text{if } T_t < T_{min,p} \\ \frac{T_t - T_{min,p}}{T_{minopt,p} - T_{min,p}}, & \text{if } T_{min,p} \leq T_t < T_{minopt,p} \\ 1, & \text{if } T_{minopt,p} \leq T_t \leq T_{maxopt,p} \\ \frac{T_{max,p} - T_t}{T_{max,p} - T_{maxopt,p}}, & \text{if } T_t \leq T_{max,p} \\ 0, & \text{if } T_t > T_{max,p} \end{cases} \quad (15)$$

where, $T$ refers to daily temperature, $min$ and $max$ refer to the minimum and maximum tolerated temperatures for growth, $minopt$ ~~(~~and $maxopt$ ~~) = minimum~~ refer to minimum and maximum optimum temperatures for growth, respectively.

### 2.1.3 Below-ground production

The root distribution, and root mass of vascular PFTs are mapped to the layout of the model's soil horizon representation (depth, density, layer thickness). To account for differences in decomposition rates among roots, and exudates, each PFT has designated SOM pools, which are partitioned between the soil layers. Root distribution, and root mass decrease exponentially from the surface to the PFT maximum root depth (MRD in Table 1). In general, 30%, 50%, and 75% of roots are observed in the top 10 cm, 20 cm, and 40 cm, respectively (**?**). Root exudation plays an important role in the rhizosphere by promoting methanogensis and soil carbon loss through $CH_4$production. The production of new roots ($Rd$) is based on a PFT prescribed shoot to root growth ratio and NPP. Root exudates ($RX$, Eq. 19) are a fraction of calculated below-ground root production ($Rd$). Exudates develop at a prescribed rate per PFT, dependent on root and shoot growth. Photosynthesis rates are enhanced during spring and summer and are accompanied by the highest levels of root and soil respiration (**?**). There is strong evidence to suggest that enhanced photosynthesis fuels exudate production, causing seasonal variation in exudation (**??**). The root growth and die off functions are adapted from van Huissteden et al. (2006).

$$Rd_{t,v,z} = (1 - RS_v) \cdot NPP_{t,v} \cdot f(z,p) \tag{16}$$

where, 1 - $RS$ represents the fraction of growth that is root growth, $f(z,p)$ [$m^{-1}$] represents the exponential root distribution from the surface to maximum root depth (MRD in Table 1).

$$\int_{-MRD_p}^{0} f(z,p)dz = 1 \tag{17}$$

$$\frac{\delta}{\delta t} RM_{t,v,z} = Rd_{t,v,z} - RX_{t,v,z} - RDR_{t,v,z} \tag{18}$$

where, $RM$ is the root mass [kg C $m^{-2}$]. $Rd$ represents the growth of new roots [kg C $m^{-2}$ $day^{-1}$], $RDR$ represents the death of existing roots [kg C $m^{-2}$ $day^{-1}$].

$$RX_{t,v,z} = Rd_{t,v,z} \cdot f(KSP_{v,DoY}) \cdot REX_{t,v} \tag{19}$$

where, DoY represents the day of the year, $REX$ represents the unitless root exudation factor, and $f(KSP)$ [-] is a function depending on PFT constant, KSP (Table 1), that can be used to determine stronger exudation occurs during spring.

$$RDR_{t,v,z} = RM_{t,v,z} \cdot RSX_v \tag{20}$$

where $RSX$ represents the root senescence rate [$day^{-1}$].

### 2.1.4 Litter layer production and decomposition

Vegetation composition change directly impacts litter inputs, which alters the quality and quantity of fresh SOM contributions (**?**). Senescence of the above-ground living biomass is added to the litter layer, for vascular PFTs (Eq. 21). Senescence of moss PFTs contributes directly to the below-ground SOM pools. Movement of surface litter to SOM pools, is an important component of peatlands (**?**). Carbon dioxide produced from the decomposition of the litter layer and the different SOM pools are summed with NEE (Eq. 4).

$$\frac{\delta}{\delta t} LL_{t,v} = LLp_{t,v} - LLl_{t,v} - LLd_{t,v} \tag{21}$$

where,

$$KT \cdot LC_p \cdot LL_{t,v} \tag{23}$$

$$LLp_{t,v} = BS_v \cdot CB_{t,v} LLl_{t,v} \quad = \quad KT \cdot LC_p \cdot LL_{t,v}$$

$$LLd_{t,v} = LL_{t,v} \cdot e^{ke_L}$$

where, $LLp$ [kg C m$^{-2}$ day$^{-1}$] refers to litter production, $LLl$ [kg C m$^{-2}$ day$^{-1}$] refers to litter lost to below-ground SOM, and $LLd$ [kg C m$^{-2}$ day$^{-1}$] refers to decomposed litter. Biomass senescence, $BS_p$ [day$^{-1}$], is set to $KL_p$ [day$^{-1}$] during Autumn, for deciduous plants (Table 1), $LC$ [day$^{-1}$] is the fraction of litter converted to SOM each day, $KT$ [°C ] is the reference temperature and T [°C ] represents the daily air temperature. Litter does not decompose if the daily temperature falls below zero. $ke_L$ [kg C m$^{-2}$ day$^{-1}$] refers to the rate of litter decomposition, adjusted by an environmental correction factor (Eq. S18, van Huissteden et al. (2006)).

### 2.1.5 Below-ground SOM decomposition

Peatlands consists of organic compounds at different stages of decomposition. In the model, these below-ground organic components are separated into five SOM pools (peat, humus, microbial biomass, litter & dead roots, root exudates, (Table S2). Each of the SOM pools lose and gain mass, whilst the number and the thickness of soil layers remain constant throughout the model simulation. Biodegradation of SOM leads to the mineralisation of carbon that can be reincorporated into SOM and repeatedly recycled (**?**). This means that some SOM pools are active (microbial biomass, litter & dead roots, root exudates) whilst others are inert (humus, peat). Active carbon pools are available for microbial decomposition and then partitioned between $CO_2$ and $CH_4$, where, inert carbon pools decompose very slowly. Inert carbon from all other SOM pools is moved

into the peat SOM pool. Vascular plants generally have faster decomposition rates than mosses (**?**) and therefore vascular plants contribute to only one of the two inert SOM pools (humus, Table S2) whereas moss PFTs contribute to both inert SOM pools (humus and peat). The decomposition of each SOM pool is calculated, assuming first order rate kinetics:

$$\frac{\delta}{\delta t} Q_{t,p,z,s} = -ke_{t,s} \cdot Q_{t,p,z,s} \tag{24}$$

where, SOM pools are represented by the subscript, $s$, $Q$ [kg C m$^{-3}$] represents the mass of organic carbon in each SOM pool, $ke$ [day$^{-1}$] represents the rate of decomposition rate for each SOM pool, adjusted by an environmental correction factor (Eq. S18, van Huissteden et al. (2006)).

$$SD_{t,p,z} = \sum_{s=1}^{S} (ke_{t,s} \cdot Q_{t,p,z,s}) \tag{25}$$

where, $SD$ [kg C m$^{-3}$] represents the total carbon lost from all SOM pools. A fraction of the decomposed carbon from the SOM pools (litter & dead roots, root exudates, peat) is transferred (mineralised and reincorporated) into microbial biomass and humus, and the remaining fraction of SD is transferred into $CO_2$. The $CO_2$ flux from the decomposition of SOM is calculated, per soil layer:

$$B_{CO_{2,t,p,z}} = SD_{t,p,z} \cdot (1 - FMI_{p,z} - HU_{p,z}) + Rox_{t,p,z} \tag{26}$$

$$FMI_{p,z} = \frac{1 - HU_{p,z}}{1 + MI_{p,z}} \tag{27}$$

where, $FMI$ [-] refers to the fraction of SOM transferred to the microbial biomass pool, calculated using PFT parameter, $MI$ [-] (Table 1), $HU$ [-] refers to the fraction of SOM transferred to the resistant humus pool, $Rox$ [kg C m$^{-2}$] represents the portion of $CH_4$ oxidised to $CO_2$ (~~maximum) optimum water level.~~ Eq. S25).

## 2.2 ~~processes~~

~~The~~

### 2.1.1 Methane processes

The net $CH_4$ flux (Eq. 28) is the sum of plant transported $CH_4$ ($Qpl$, Eq. 29) and the below-ground processes: anaerobic $CH_4$ production ($Rpr$), $CH_4$ oxidation ($Rox$), ebullition ($Qeb$), and diffusion of $CH_4$ through soil ($Fdiff$). The ~~soil layer is subdivided into 15 layers of equal thickness (0.1 m) and the flux rate~~ flux of each layer is calculated before integrating over all layers to obtain the total $CH_4$ flux. These $CH_4$ process were adapted from the Peatland-VU model ~~described in~~

?van Huissteden et al. (2006). (van Huissteden et al., 2006), originally described in ?.

$$\frac{\delta}{\delta t}C_{CH_4,t,z} = Rpr_{t,z} - \sum_{p=1}^{P}(Qpl_{t,p,z}) - \frac{\delta}{\delta Z}\frac{\delta}{\delta z}Fdiff_{t,z} + - Qeb_{t,z} + Rpr_{t,z} + - Rox_{t,z} \quad (28)$$

Where $C_{CH_4}$ represents the $CH_4$ concentration [$\mu$M m$^{-3}$]at time, t and depth z, , $Qpl$ [$\mu$M m$^{-3}$ day$^{-1}$] is the $CH_4$ flux by plant roots Eq. 29, $Fdiff$ [$\mu$M m$^{-2}$ day$^{-1}$] is the diffusive flux (Eq. S20). $Qeb$ [$\mu$M m$^{-3}$ day$^{-1}$] represents ebullition of $CH_4$, (Eq. S23). $Rpr$ [$\mu$M m$^{-3}$ day$^{-1}$] is the temperature dependent production of $CH_4$ by anaerobic peat oxidation , and (Eq. S24), where warmer temperatures lead to enhanced $CH_4$production rates (?). $Rox$ [$\mu$M m$^{-3}$ day$^{-1}$] is the temperature dependent removal of $CH_4$ by methanotrophic oxidation of $CH_4$ to $CO_2$ in the soil .

The PVN model has adapted the plant transport pathway so that plant (Eq. S25), where warmer temperatures lead to enhanced $CH_4$oxidation rates (?). The diffusive flux, $Fdiff_{t,z}$ is calculated using Fick's first law (Sect. 1.3.1).

Plant transported $CH_4$ is calculated for each PFT. Anaerobic $CH_4$ production, ebullition and diffusion of $CH_4$ through the soil remain as described in ?van Huissteden et al. (2006)van Huissteden et al. (2006), originally adapted from Walter et al. (2001)?. There are two mechanisms which determine the amount of $CH_4$ lost via plant transport. Firstly, the spread and density mass and distribution of the root system plays a role in determining how much $CH_4$ is taken up into the plant tissue. Thereby, a dense or large root system enables , along with enhanced soil concentrations, more $CH_4$ to enter the plant tissue. When $CH_4$passes through the oxic zone around the root tips, a fraction of $CH_4$consumed by rhizospheric oxidation (?). This is represented by the unitless PFT parameter, $PlOx$ (Eq. 30). Secondly, the amount of $CH_4$ transported through the plant tissue and released to the atmosphere is determined by its aerenchyma. Plants with (without) large aerenchyma are (in)efficient transporters of $CH_4$. The unitless parameter MethanePlantOx_PFT ($PlOx$ in ) is used to delineate PFT parameter. $vP$ [-], describes the plant's capacity ability to conduit $CH_4$.

$$Qpl_{t,p,z} = -cP \cdot vP_p \cdot LAI_{t,p} \cdot RD_{t,p,z} \cdot C_{CH_4,t,z}$$

where, $RD$ is a function representing the distribution of roots per soil layer through above-ground plant tissue (Table 1). Shrubs and trees generally do not have aerenchyma whereas, grasses and sedges can have large or small aerenchyma (Ström et al., 2005; ?). The values for these PFT parameters are taken from the literature and are cited in Table S3.

$$Qpl_{t,p,z} = -cP \cdot vP_p \cdot LAI_{t,p} \cdot f(z,p) \cdot C_{CH_4,t,z} \quad (29)$$

where, $cP$ represents the site specific constant [day$^{-1}$] and $vP$ represents the unitless PFT rate constant , MethanePType_PFTis a rate constant with a value of 0.24 (taken from ?), $f(z,p)$ [m$^{-1}$] represents the exponential root distribution (Eq. 17) (van Huissteden et al., 2006; ?). The rate of plant transported $CH_4$ is integrated over the depth of the root zone to obtain

the flux at the surface (Eq. 30).

$$Fpl_{t,p,z} = \int_{z}^{0} \left[ Qpl_{t,p,z} \cdot (1 - PlOx_p) \right] dz \tag{30}$$

where, $Fpl$ represents the total plant transported $CH_4$ flux [$\mu$M day$^{-1}$].

### 2.1.2 ~~processes~~Harvest scheme

~~At the beginning of each day, C3 photosynthesis (), leaf respiration ($RE$), and net primary production (NPP) are calculated using modified versions of the primary production scheme introduced in ?, modified from Haxeltine et al. (1996). The net fluxes for each PFT (NEE, ) are the sum of photosynthesis minus plant respiration, the production of by below-ground aerobic decomposition of inert SOM ($KCO_2$, kg C m$^{-2}$), and the portion of oxidised from ($Rox$).~~

$$NEE_{t,p} = AP_{t,p} + \int_{z}^{0} B_{CO_{2,t,p}} dz - \int_{z}^{0} RT_{t,p} dz$$

~~where, $NEE$ is the Net Ecosystem Exchange kg C m$^2$, $AP$ is the daily potential photosynthesis calculated in kg C m$^{-2}$, $B_{CO_2}$ is the flux produced by below-ground SOM decomposition kg C m$^{-3}$(), and $RT_{t,p}$ is the daily plant respiration kg C m$^{-2}$~~If the harvest scheme is activated in the model input file, PFTs taller than the prescribed harvest height are harvested (mowed) at the prescribed date. This is a relevant feature for agricultural (e.g. Knox et al. (2015)) or other managed peatlands (e.g.

$$AP_{t,p} = FPAR_{t,p} \cdot \sigma \cdot \phi \cdot PAR \cdot AI_{t,p} \cdot fG_{t,p}$$

~~where $FPAR$ is the fraction of incoming $PAR$ J m$^{-2}$ day$^{-1}$absorbed by vegetation () , $AI$ represents total daily incident PAR gC m$^{-2}$ day$^{-1}$, $\phi$ is the quantum efficiency of gross photosynthesis at prescribed ambient M-C M-photons$^{-1}$, $fG$ is a unitless temperature stress scalar dependent on favourable air temperatures and incoming solar radiation, $\sigma$ is a dimensionless factor that depends on the fractional day length ($TD$) :~~

$$\sigma = \sqrt{1 - \frac{a_{t,p}}{TD_t}}$$

~~where, $a$, the ratio of leaf respiration to photosynthetic capacity (we used the ratio value, 0.08, taken from Haxeltine et al. (1996)).Instantane photosynthesis ($AI$) is calculated by:~~

$$AI_{t,p} = \frac{\phi \cdot I \cdot A_{max,t,p}}{\phi \cdot I_{t,p} + A_{max,t,p}} - RE_{t,p}$$

where, $I$ is the instantaneous PAR flux J $m^{-2}$ $s^{-1}$, $A_{max}$ is the maximum rate of photosynthesis J $m^{-2}$ $s^{-1}$, and $RE$ is the instantaneous rate of leaf respiration gC $m^{-2}$ $s^{-1}$.

$$RE_{t,p} = R_p * fG_{t,p}$$

where, where, $fG$ is a unitless temperature stress scalar dependent on favourable air temperatures and incoming solar radiation, and $R$ is the leaf respiration constant g C $m^{-2}$ $s^{-1}$?).

### 2.1.3 Below-ground SOM decomposition

Each below-ground SOM pool (peat, labile organic matter, exudates, microbial biomass, litter & dead roots, root exudates)is partitioned between active and inert carbon pools, where the active carbon pool is available for microbial decomposition and then partitioned between $CO_2$ and $CH_4$. Non-moss PFTs do not contribute to the storage of peat. The decomposition of soil layers that lie beneath the water level are calculated, assuming first order rate kinetics:

$$\frac{\delta Q_{t,p,z}}{\delta t} = -k_p \cdot Q_{t,p,z}$$

where, Q is the mass of organic C in each SOM pool kg C $m^{-3}$, and k is the decomposition rate $day^{-1}$for each SOM pool. The flux from each SOM pool is calculated as:

$$B_{CO_2,t,p,z} = \frac{\delta Q_{t,p,z}}{\delta t} \cdot (1 - MI_{t,p,z} - HU_{t,p,z})$$

where, $MI$ kg C $m^{-2}$refers to SOM transferred to the microbial biomass pool and $HU$ kg C $m^{-2}$refers to the SOM transferred to the resistant humus pool. The remaining fraction of $\frac{\delta Q_{t,p,z}}{\delta t}$ is transferred into . harvest height and days are therefore, optional prescribed model parameters. Living biomass decreases according to the amount of biomass harvested because biomass is assumed to be uniformly distributed with height and is not partitioned into organs. LAI is recalculated (Eq. 8) and the PFT height is set to the harvested height. A fixed fraction of the harvested material remains uncollected in the field and is added to the litter layer.

### 2.1.3 Below-ground production

Root exudation plays an important role in the rhizosphere by promoting methanogensis and soil carbon loss through production. The production of new roots ($Rd$) is based on a PFT prescribed shoot to root growth ratio and NEE. Root exudates ($RX$, ) are a fraction of calculated below-ground root production ($Rd_{p,z,t}$). Exudates develop at a prescribed rate per PFT which is

dependent on root and shoot growth.

$$\frac{\delta}{\delta t} RM_{t,p,z} = Rd_{t,p,z} - RX_{t,p} - RDR_{t,p}$$

where, $RM$ is the root mass kg C $m^{-2}$at time t, and soil depth z. $Rd$ represents the growth of new roots kg C $m^{-2}$ $day^{-1}$, $RDR$ represents the amount of death of existing roots kg C $m^{-2}$ $day^{-1}$.

$$RX_{t,p,z} = Rd_{t,p,z} \cdot FSP_{p,DoY} \cdot REX_{t,p}$$

where, DoY represents the Julian day of the year, $REX$ represents the unitless root exudation factor so that maximum exudates occurs during spring ($FSP_{p,DoY}$) .

$$RDR_{t,p,z} = RM_{t,p,z} \cdot RSX_p$$

where $RSX$ represents the root senescence rate $day^{-1}$.

$$Rd_{t,p,z} = \frac{\delta}{\delta t} RM_{t,p,z} \cdot NPP_{t,p} \cdot (1 - RS_p)$$

where, $RS$ is a PFT shoot to root growth ratio -.

### 2.1.3 Litter layer production and decomposition

Senescence of the above-ground living biomass is added to the litter layer, for non-moss PFTs. Senescence of moss PFTs contributes directly to the below-ground SOM pools:

$$\frac{\delta}{\delta t} LL_{t,p} = (1 - KB_p) \cdot CB_{t,p} - \frac{KL_p}{KT} \cdot T_t$$

where, leaf senescence, $KB_p$ $day^{-1}$, is set to 0.05 during Autumn, $KL_p$ represents the fraction of leafy biomass littered during Autumn $day^{-1}$, $KT$ is the reference temperature and T represents daily air temperature .

All model code has been written in C++. The model code is publicly available from the Bitbucket repository (, last accessed 10 January 2023) under the GNU General Public License version 3, or any later version. Users are welcome to contact the authors for technical support. The model schematic in was composed in Adobe Indesign. All other figures in this manuscript were plotted using Python and particularly the pandas, Seaborn and Matplotlib libraries.

## 2.2 Two peatland sites

With this study, the PVN model simulates two peatland sites~~in the Netherlands~~, the Horstermeer site and the Ilperveld site (Fig. S1). The Ilperveld site (52°26' N, 4°56' E; 1.42 meters below sea level (mbsl)) is currently a nature recreation area that is a former raised bog complex that was drained to be used as agricultural pasture, and frequently exposed to manure fertilisation (van Geel et al., 1983; Harpenslager et al., 2015). Since the early 2000's, the Ilperveld site has undergone restoration efforts which included raising the water level, removal of the fertilised & ~~nutrient rich~~ nutrient-rich top soil, attempts to re-introduce *Sphagnum*, and water quality management. The vegetation consists of brown mosses, *Sphagnum*, and grasses (*Poaceae* family). Since restoration began, the site has been mown twice a year, in June and September. Vegetation profiles show layers of intact *Sphagnum*/*Carex* peat and unlike undisturbed peatlands, the top layer has undergone greater decomposition due to land management since drainage (Harpenslager et al., 2015). The Horstermeer site (52°15' N, 5°04' E; 2.1 mbsl) lies on the Horstermeer polder and is a former drained agricultural peat meadow that has not been used since the 1990s when the water level was also raised. It was used for grazing and exposed to manure fertilisation until the 1990s. The Horstermeer site is now a semi-natural fen containing very heterogeneous vegetation, including reeds, grasses, and small shrubs, and is not subject to mowing or other land management practices (Hendriks et al., 2007). Vegetation consists of different types of grasses and sedges (dominant species *Holcus lanatus*, *Phalaris arundinacea*, *Glyceria fluitans*), and reeds (*Phragmites australis*, *Typha latifolia*). The Horstermeer polder is subject to strong seepage of mineral rich groundwater from surrounding lake areas and Pleistocene ice pushed ridges (Hendriks et al., 2007). The Horstermeer polder was a freshwater lake that was drained as part of large-scale land reclamation project completed in 1888.

### 2.2.1 ~~PFT attributes~~

## 2.3 PFT attributes

This study defined six PFTs (*Typha*, sedges, tall grasses, short grasses, *Sphagnum*, brown mosses) based on the vegetation communities observed at the Horstermeer and Ilperveld sites. PFT attributes (Table ~~??~~1) were amalgamated from the NUCOM-BOG model, the TRY 5.0 database (https://www.try-db.org, last accessed 18 May 2022) (Kattge et al., 2011, 2020) and other relevant publications listed in Table S3. As much as possible, PFT parameter values are informed by observational data (i.e. Kattge et al. (2011, 2020); Heijmans et al. (2008)). Sedges, tall grasses and *Typha* all represent graminoids with deep root systems that can grow at a range of water levels but have different aerenchyma and growing ranges. Sedges are from the family *Cyperaceae* and *Juncaceae* and are grass-like, monocotyledonous flowering plants with aerenchymae. Tall grasses are from the family *Poaceae* and are grass-like plants with elongated long blade-like leaves without aerenchyma. *Typha* PFTs represent a genus of about 30 species of monocotyledonous flowering plants in the family *Typhacea* with large aerenchyma. The short grasses PFT is representative of forbs and agricultural-like grasses with shallow root systems. The *Sphagnum* PFT is representative of hummock *Sphagnum* species which are generally more drought tolerant. Brown mosses represent all non-*Sphagnum* mosses but have similar but slightly broader temperature growth ranges. The SOM evolved from short grasses decomposes more easily than SOM evolved from brown mosses which decomposes more easily than SOM evolved

from *Sphagnum*. The six PFT input ~~parameters~~ parameter sets used in this study are accessible from the bitbucket repository, bitbucket.org/tlippmann/pvn_public.

~~Plant functional type parameters and bioclimatic limits. The parameter definitions are listed in 1. Associated references are listed in S3. Parameter Units Tall grass Sedges *Typha* *Sphagnum* Brown moss Short grass BiomassSenescence - 0.04 0.04 0.04 0.01 0.015 0.03 AutumnLitter - 0.1 0.1 0.1 0.01 0.04 0.06 CBiomassRatio $kgC kgC^{-1}$ 0.46 0.46 0.46 0.44 0.44 0.44 ShootsFactor - 0.7 0.7 0.7 1.0 1.0 0.9 MaxCanopyHeight m 1.5813 2.5813 2.5813 0.1 0.2 0.2 Temp_MaxPhoto °C 38 40 35 30.0 30.0 30 Temp_MinPhoto °C -3 -1 -3 -1.0 0.5 -1 TMinGrowth °C 7 2 2 -1.0 0.5 0.5 TOptMinGrowth °C 9 12 12 14.0 5.0 14 TOptMaxGrowth °C 20 30 30 25.0 25.0 25 TMaxGrowth °C 45 45 45 38.0 38.0 38 LeafRespirationCoeff - 0.015 0.015 0.015 0.016 0.014 0.014 MaxGrowthRate $gC day^{-1}$ 0.07 0.07 0.07 0.045 0.05 0.05 SpecificLeafArea $m^2 g^{-1}$ 0.012 0.012 0.012 0.02 0.02 0.02 MinLAI $m^2 m^{-2}$ 0.1 0.1 0.1 0.1 0.1 0.1 MaxLAI $m^2 m^{-2}$ 3 4 4 1.2 1.5 1.5 LightExtCoeff - 0.5 0.46 0.5 0.95 0.95 0.95 MethanePlantOx - 0.4 0.4 0.25 0.7 0.8 0.6 MethanePType - 5 6 10 2.0 2.0 2 MaxRootDepth m 0.46 1 1 0.1 0.1 0.2 RootSenescence $day^{-1}$ 0.05 0.05 0.05 0.04 0.04 0.05 ExudateFactor - 0.1 0.2 0.2 0.05 0.1 0.11 SpringCorrection - 0.2 0.4 0.4 0.0 0.0 0.1 LitterConversion $day^{-1}$ 0.005 0.001 0.001 0.01 0.005 0.003 ResistFrac - 0.55 0.42 0.3 0.9 0.9 0.9 AssimDissim - 2.25 2.2 2.2 2.4 2.3 2.3 WLMin m -1 -1 -1 -0.5 -0.35 -0.35 WLOptMin m -0.4 -0.3 -0.4 -0.2 -0.15 -0.15 WLOptMax m -0.2 -0.2 0 -0.05 -0.05 -0.05 WLMax m 0.0192 0.1 0.3 0.05 0.05 0.05~

### 2.3.1 ~~Model calibration~~

## 2.4 Model calibration

The model was calibrated to reproduce fluxes that fall within the spread of observed in situ chamber measurements, measured at the Horstermeer and Ilperveld peatland sites (~~described in~~ Sect. 2.2). The PVN model simulates processes on a daily time step. We ran the model using twenty eight years (1990 - 2017, inclusive) of input data (Sect. 2.7) for the Horstermeer and Ilperveld sites. The length of the model spin-up was five years, determined by the time taken for the SOM pools, below-ground $CO_2$ and below-ground $CH_4$ concentrations to stabilise. Thereby, the first five years of model simulations (1990 - 1995) are considered as the spin-up period. Daily $CO_2$ and $CH_4$ fluxes measured at the Horstermeer and Ilperveld sites between 2015 and 2017 were used to calibrate the model. Unfortunately there was not enough data to split the observational data into separate datasets for calibration and validation.

A Monte Carlo analysis was performed separately for each site to calibrate ~~the model input parameters . Since the~~ thirteen model parameters (Table. S4). Parameters without available observational data were included in the model calibration process. The Kling-Gupta efficiency (KGE) metric was used to measure the agreement between simulated and observed $CO_2$ and $CH_4$ fluxes (**??**). The KGE approach is a three dimensional decomposition of the Nash-Sutcliffe efficiency (NSE) measure and evaluates temporal dynamics, bias, and variability Eq. 26. The KGE metric has been used to assess the ability of carbon flux models (**??**), hydrological models (**?**), and meteorolgical reanalysis datasets (**??**) to reproduce in situ observations. The calibrated model input values are provided in Table S6 and Table S7 for the Horstermeer and Ilperveld site simulations, respectively.

**Table 2.** A summary of the varied input data used to understand the sensitivity of the model. *To compare the PFT dynamics, both simulations use the 'no harvest' regime. The exchange of PFTs means that the model simulation driven by the Ilperveld input data (Table 4) will use the PFTs observed at the Horstermeer site (*Typha*, tall grass, sedges, brown moss PFTs) while the model simulation driven by the Horstermeer input data (Table 4) will use the PFTs observed at the Ilperveld site (short grass, tall grass, *Sphagnum*, brown moss PFTs).

| Changing input variable | Input change |
|---|---|
| Air temperature | $\pm 1$ °C, $\pm 3$ °C |
| Harvest frequency | no harvest; once, twice, three, and four times per year |
| PFTs | Exchange Ilperveld and Horstermeer PFTs* |
| Radiation | $\pm 8$ J m$^{-2}$, +100 J m$^{-2}$, +200 J m$^{-2}$ |
| Water level | $\pm$0.1m, $\pm$0.2m |

The $CO_2$ results impact the $CH_4$ results much more than the $CH_4$ results impact the $CO_2$ results, therefore we first ensured that the parameters impacting the photosynthesis, and above and below ground growth and respiration schemes reproduced fluxes that fell within the spread of observed $CO_2$ fluxes (NEE). These were the MolAct, HalfSatPoint, VegTScalingFactor parameters. Next, the $CH_4$ scheme was calibrated to reproduce fluxes that fell within the spread of observed $CH_4$ fluxes. This involved calibrating the remainder of the parameters highlighted in Table. S4. Even though the amount of photosynthesis and living biomass does not directly impact the $CH_4$ production, which primarily occurs in the soil and above-ground litter layers, these processes are precursors to root and shoot growth, respiration, and senescence, which directly impact simulated $CH_4$ fluxes. After optimisation of the $CH_4$ fluxes, the PFT parameters ( Table S3) were manually adjusted to bring the PFT ~~BF~~ biomass fractions (PFT biomass as a fraction of total biomass) in line with observed aerial cover fraction ratios. ~~These adjusted parameters are described as being an adapted parameter in Table S3.~~ The calibrated model parameters and the necessary input files used to simulate the two peatland sites evaluated in this study are accessible from the bitbucket repository, bitbucket.org/tlippmann/pvn_public.

### 2.5 Testing the PVN model

To understand the sensitivity of net $CO_2$ and $CH_4$ fluxes to PFT dependent processes, we conducted several model simulations using modified input data. We tested the sensitivity of PFTs processes to air temperature, water level, radiation, and harvest schemes by varying these inputs one by one (~~summmarised in~~ Table 2).

To understand how the new model mechanisms affect emissions, we performed additional simulations with altered model algorithms and compared these to the original model simulations calibrated for the Horstermeer and Ilperveld sites (Table 3). For example, the contribution of competition for shading to the overall simulation result, is quantified by comparing an altered simulation where incoming ~~photactive~~ photosynthetically active radiation (PAR) is independent of shading (e.g. fractional par or FPAR = 0.25 for a simulation with four PFTs) to the original model simulations (FPAR_CONST). We calculated the relative difference of the simulation with shading minus the simulation without shading. Similarly, we compared simulations with and without plant transported $CH_4$(CH4_OLD_CF), with and without dynamic BF (CF_CONST), with and without variable ~~height~~plant height (HEIGHT_CONST).

**Table 3.** A summary of the simulations with altered model algorithms.

| Simulation name | Mechanism change |
|---|---|
| CH4_OLD_CF | Uses Peatland-VU $CH_4$ module multiplied by the PFT cover fraction |
| CF_CONST | Biomass fraction is constant for all PFTs, i.e. BF = 0.25 |
| FPAR_CONST | FPAR is constant for all PFTs, i.e. FPAR = 0.25 |
| HEIGHT_CONST | Constant plant height for each PFT |

In order to demonstrate that the PVN model reproduces $CH_4$ and $CO_2$ fluxes within the spread of observed fluxes when driven by realistic input data, we compared the ~~modeled~~ calibrated model simulation results and measured $CH_4$ and $CO_2$ fluxes for ~~two sites,~~ the Horstermeer and the Ilperveld field sites ~~, in North Holland, the Netherlands~~ (Sect. 2.2).

We compare the $CH_4$ and $CO_2$ fluxes ~~simulated by the new PVN model~~ of the calibrated model simulation results against the $CH_4$ and $CO_2$ fluxes simulated by the Peatland-VU model to understand the impact of introducing PFTs on the simulation of $CH_4$ and $CO_2$ fluxes. These model simulations are summarised in Table 4. Attempts to run the Peatland-VU model with new calibrated parameters did not yield results in the same order of magnitude as the observations. Therefore, it was necessary to use different model parameterisations for the PVN and Peatland-VU models.

### 2.6 Flux measurements

Carbon dioxide and $CH_4$ fluxes were measured using 2-4 automated flux chambers (AC) and the Ultra-Portable Los Gatos Gas Analyser ~~, aligned with standardised chamber technique measurement protocol (Pavelka et al., 2018)~~Model 915-001. Chambers were cylindrical, 30cm wide and 40cm in height, made of transparent acrylate, equipped with a fan and installed in the field using collars. Where necessary, vegetation was folded gently to fit inside the measurement chambers. Collars were removed from the field between sampling campaigns which minimises disturbance which can lead to potential biases in the observations. This also potentially introduces uncertainty as to the precise measurement location. The $CO_2$ and $CH_4$ concentrations were measured for 150 second intervals, whilst the chamber was closed. Each chamber was measured on rotation so that a new chamber was measured every 15 minutes. Measurements were recorded ~~24~~ continuously, during the day and night, for a week at a time, upon which the AC system was moved to another site. We note that due to the labor intensive nature of accumulating chamber observations consistently through time, these observational datasets do not offer complete temporal continuity, creating an intermittency bias. ~~The and concentrations were measured inside the chamber, whilst the chamber was closed, during 15 minute intervals.~~ From this data, the ~~daily~~ hourly average $CO_2$ (net ecosystem exchange) and $CH_4$ fluxes were calculated ~~. To evaluate the model, we compared simulated and observed daily hourly~~ for each day. We compared calibrated site simulations against observed daily average $CO_2$ and $CH_4$ fluxes. To ~~estimate the degree of uncertainty, daily~~ visualise the daily variability, standard deviations were derived from the hourly fluxes. The values for all GHG emissions are expressed as $CO_2$ equivalents ($kgCO_{2eq}m^{-2}yr^{-1}$) and calculated as

$$GHG_{CO_2e} = CH_4 \cdot GWP + CO_2 \tag{31}$$

where,

$GWP_{20}$ = 80.8, as 1 $kgCH_4$ = 80.8kg $CO_2$eq, over a 20 year time horizon, and

$GWP_{100}$ = 27.2, as 1 $kgCH_4$ = 27.2 kg $CO_2$eq, over a 100 year time horizon (**?**).

## 2.7 Input data preparation

The PVN model is driven by daily air temperature ($T$), water level (WL), radiation, a general model parameter input file (Table. S4), and a soil parameter input file (Table S5).

### 2.7.1 Climatological input data

Daily temperature and radiation data, measured at Schiphol, the nearest KNMI weather station was used as climate input data for both sites (accessed via https://www.knmi.nl/nederland-nu/klimatologie/daggegevens, last accessed 18 May 2022) (Fig. S3). The annual average rainfall at Schiphol, was 850 mm $yr^{-1}$ over the period, 1990-2020, with 30% of the rainfall falling in summer and autumn, respectively, and 24% falling in winter, with the remainder falling in the spring. The average daily temperature between 1990 and 2019 was 9.4 °C and warmed approximately +0.1 °C$yr^{-1}$ over the same period. The average daily temperature for the warmest month, August, was 22.1 °C and the lowest daily monthly temperature for the coldest month, January, was 0.8 °C.

### 2.7.2 Soil profile input data

The model generates a soil horizon representation using soil layers of 10cm thicknesses. The generated soil horizon uses properties such as dry bulk density (DBD), SOM ratio, sand content, C:N ratio specified in the soil profile input data (Table S5). The number and depth of the site's soil horizons can be adjusted in the soil input file. The PVN model requires input parameters for each PFT, discussed in Section 2.3. Soil profile data from the Horstermeer and Ilperveld field sites was collected in 2015 and 2016 and includes DBD, C content, SOM content, sand and clay content, pF curve ~~.~~ (Table S8 and Table S9, for the Horstermeer and Ilperveld site simulations, respectively).

### 2.7.3 Water level input data

Water level input data was sourced from the Dutch hydrological model, Netherlands Hydrological Instrument (NHI) (De Lange et al., 2014)~~.~~, which has a reasonably high spatial resolution (250m x 250m). One aim of developing the PVN model is to eventually develop a model of all Dutch peatlands in conjunction with the NHI product. For this reason, the NHI product is used in this application of the model. The NHI water level output was converted to relative surface height using ~~the~~ a 5m x 5m digital elevation map of the Netherlands, Actueel Hoogtebestand Nederland (Alhoz et al., 2020). ~~The required input data for both peatland~~ It is possible to use in situ water levels as input data for the model but this data was unfortunately, unavailable for the duration of the simulation. The input data used for both sites is accessible from the bitbucket repository, bitbucket.org/tlippmann/pvn_public.

**Table 4.** A summary of the model simulations, using both the new PVN model and the pre-existing Peatland-VU (PV) model. PVN is an alphabetisation for the Peatland-VU-NUCOM v1.0 model. PV is alphabetisation for the Peatland-VU model. Model input parameters for the Horstermeer and Ilperveld site simulations are provided in Table S6 and Table S7, respectively.

| Site | Model | Vegetation | Harvest height~~Soil Profile WL Input~~ |
|---|---|---|---|
| Horstermeer | PVN | *Typha*, sedges, tall grass, brown moss | - ~~Horstermeer Horstermeer~~ |
| Horstermeer | PV | - | - ~~Horstermeer Horstermeer~~ |
| Ilperveld | PVN | Short grass, tall grass, brown moss, *Sphagnum* | 0.15m ~~Ilperveld Ilperveld~~ |
| Ilperveld | PV | - | 0.15m ~~Ilperveld Ilperveld~~ |

## 3 Results

The sign convention in this paper is that a positive gas flux is indicative of the flux entering the atmosphere and a negative flux is indicative that the flux is from the atmosphere. When describing ~~on~~ the annual $CO_2$, $CH_4$, and GHG values, we opt to use the term emissions, e.g. 'the total annual GHG emissions', whereas, when describing daily values, we opt to refer to these as fluxes, e.g. 'the daily GHG fluxes'. ~~The goal of this study is not to create a new peatland emissions model to outperform the Peatland-VU model but to develop a new model capable of understanding the role dynamic PFTs have on and emissions in peatlands and for this reason, we do not aim to produce a new model to outperform the Peatland-VU model but a model that uses new dynamic processes where the model skill may be comparable to that of the Peatland-VU model.~~

### 3.1 Model sensitivity to input data

To understand the response of the modeled PFT processes to input data, we ran simulations with modified water levels (Fig. 3 and Fig. S5), temperature (Fig. 2 and Fig. S4), radiation (Fig. S6) input and harvest schemes (Fig. 4). The modified input data is summarised in Table 2 and the results of these sensitivity tests are summarised in Table 5. These results are indicative of the model mechanistic responses rather than projections on how PFTs might respond under varied environmental conditions. To show how different inputs impact ~~plant~~ model processes, we present the ~~belowground~~ soil (respiration) $CO_2$ emissions (Fig. 3), plant transported $CH_4$ (Fig. 2), above-ground biomass (Fig. 4). In the PVN model, the abundance of each PFT varies through time depending on the favourability of growing conditions. Therefore, an increase in $CO_2$ or $CH_4$ fluxes may be due to increased abundance (i.e. enhanced biomass) or enhanced transport efficiency. To disentangle this difference, the $CO_2$ and $CH_4$ fluxes for each PFT are plotted as a fraction of litter and root mass.

~~Warming~~ Increased air temperatures had a positive effect on both plant transported $CH_4$ emissions (Fig. 2) and litter & root mass at both sites (Fig. S4). Short and tall grasses showed similar responses to ~~warming~~ increased air temperatures by producing large $CH_4$ emissions per kg of litter and root mass. Brown mosses showed little variation between the temperature experiments for the Ilperveld site but showed a decrease in fluxes with warming temperatures per kg of litter and root mass at the Horstermeer site. *Sphagnum* similarly showed a decrease in $CH_4$ fluxes with warming temperatures per kg of litter and root mass at the Ilperveld site. This decrease is because moss PFTs have strict ideal temperature growth limits and were limited

**Table 5.** The results of the sensitivity testing. The $CH_4$ and $CO_2$ columns indicate how much the respective emissions changed when the input changed, relative to the results of the respective default Horstermeer and Ilperveld PVN simulations described in Table 4. A dash [-] indicates the simulation is the default site simulation. An overview of the sensitivity tests can be found in 2.

| Changing input variable | Input change | Horstermeer | | Ilperveld | |
|---|---|---|---|---|---|
| | | $CH_4$ [%] | $CO_2$ [%] | $CH_4$ [%] | $CO_2$ [%] |
| Air temperature | +3°C | 165 | 117 | 115 | 122 |
| | +1°C | 128 | 94 | 102 | 108 |
| | -1°C | 77 | 93 | 100 | 87 |
| | -3°C | 56 | 66 | 154 | 53 |
| Harvest frequency | no harvest | - | - | 120 | 129 |
| | 1 $year^{-1}$ | 114 | 68 | 87 | 117 |
| | 2 $year^{-1}$ | 114 | 67 | - | - |
| | 3 $year^{-1}$ | 115 | 67 | 152 | 70 |
| | 4 $year^{-1}$ | 114 | 68 | 185 | 45 |
| PFTs | *Typha*, sedges, tall grass, brown moss | - | - | 291 | 294 |
| | Short grass, tall grass, brown moss, *Sphagnum* | 35 | 68 | - | - |
| Radiation | +200 J $m^{-2}$ | 121 | 107 | 97 | 126 |
| | +100 J $m^{-2}$ | 111 | 104 | 98 | 113 |
| | +8 J $m^{-2}$ | 101 | 101 | 98 | 101 |
| | -8 J $m^{-2}$ | 99 | 99 | 98 | 99 |
| Water level | +0.2m | 149 | 104 | 200 | 99 |
| | +0.1m | 134 | 103 | 172 | 100 |
| | -0.1m | 98 | 98 | 87 | 101 |
| | -0.2m | 163 | 97 | 281 | 101 |

by warming temperatures. Whilst ~~belowground~~ below-ground $CH_4$ concentrations increased with warming temperatures, the biomass, litter, and root mass of moss PFTs did not increase with warming temperatures.

Below-ground $CO_2$ emissions were impacted by changing water levels (Fig. S5). Previous studies have found that ~~belowground~~ below-ground $CO_2$ production tends to increase with low water levels due to enhanced potential for aerobic $CO_2$ production (Knox et al., 2015). The results of the Ilperveld site sensitivity simulations showed that ~~belowground~~ below-ground $CO_2$ production increased with low water levels, likely due to enhanced potential for aerobic $CO_2$ production. However, the results of the Horstermeer site sensitivity simulations showed the converse, that the net $CO_2$ (Table 5) and ~~belowground~~ below-ground $CO_2$ production increased with high water levels. We simulate that with high water levels, the reduced aerobic $CO_2$ production can be exceeded by the enhanced oxidation of $CH_4$ into $CO_2$. The large amounts of $CH_4$ oxidised into $CO_2$ in the Horstermeer site simulation are due to the very degraded peat present at the site (represented by low soil OM content in the soil input file)

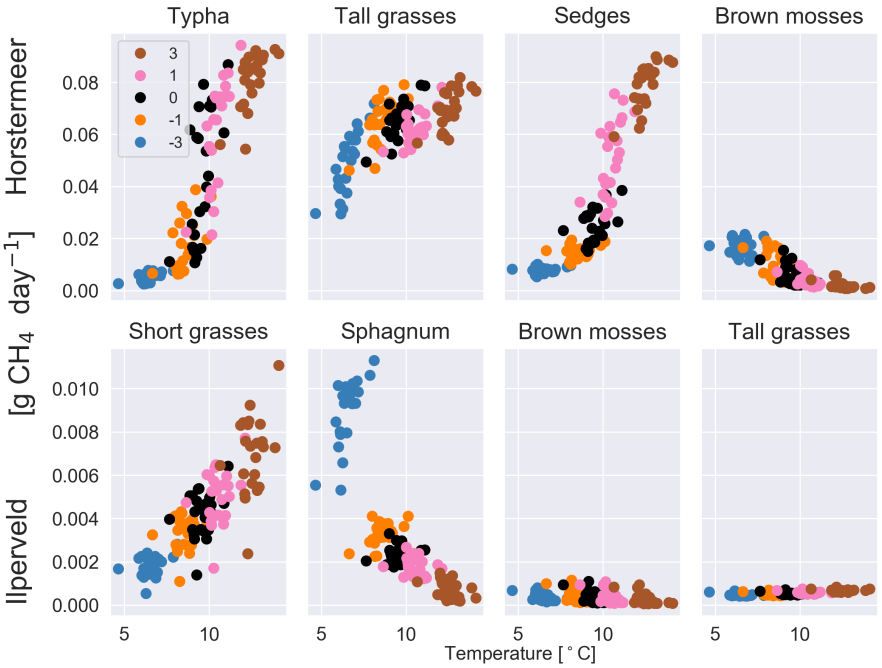


**Figure 2.** The results of the sensitivity tests show the relationship between different temperature inputs and the mean daily plant transported $CH_4$ for each year, for each of the PFTs at the Horstermeer site (top row) and Ilperveld site (bottom row). Temperature input was increased and decreased by 1 & 3 °C, respectively. The legend shows the input change in °C where, ± signs in front of the legend labels show the direction of change. Note the different y axes between the top and bottom panels.

and the strong upwelling of rich groundwater at the Horstermeer site (represented by ~~a site specific parameter~~model parameter, MolAct, which influences the sensitivity of aerobic $CO_2$ production). The large observed $CH_4$ emissions at the Horstermeer site are partially due to high $CH_4$ concentrations in the upwelling water. Furthermore, the large root systems of plants such as *Typha*, sedges and tall grasses have greater potential to access and transport stores of below-ground gases (represented by the PFT root depth and ~~density~~mass). The conflicting response of the tall grass PFT in the Ilperveld and Horstermeer simulations shows that PFTs may respond differently to changing water levels at different sites.

Increasing the frequency of harvests led to a strong negative effect on vascular plant biomass and a small positive effect on moss plant biomass (Fig. 4). Biomass of non-moss PFTs is strongly impacted by the occurrence of harvests as indicated by the pause in biomass accumulation after harvest. However, by reducing tall vegetation, moss species have greater access to sunlight and therefore, gain an advantage. For this reason, we saw the biomass of moss PFTs increase with more frequent harvests. In the Horstermeer site simulation, the greatest effect on biomass was between no harvests and the once per year harvests. In the Ilperveld site simulation, the effects of harvests on biomass increased somewhat linearly, according to the frequency of harvest events. We suspect that this is due to the inclusion of different PFTs in the two site simulations. In the Horstermeer site simulation, three PFTs have the capacity to grow above the harvest height (the *Typha*, tall grass, and sedge PFTs) whereas in the Ilperveld site simulation only tall and short grasses have the potential to grow beyond the harvest height, thereby limiting


**Figure 3.** The results of the sensitivity tests show the relationship between different water level inputs and the mean daily soil $CO_2$ flux for each year, for each of the PFTs at the Horstermeer site (top row) and Ilperveld site (bottom row). Water level input was decreased by 0.1 & 0.2 m and increased by 0.1 & 0.2 m, respectively. The legend shows the input change, where $\pm$ signs in front of the legend labels indicate the direction of change. Note the different y axes between the top and bottom panels.

the potential effect harvests can have on the PFTs present. Furthermore, the growth of the short grasses PFT is height limited to 0.3m. Overall, total biomass was reduced with more frequent harvest regimes. It's important to note that whilst $CO_2$ emissions reduced by increasing the frequency of harvests (Table 5), these emissions are not accounting for the off-site decomposition of harvested biomass.

### 3.2 Assessment of model mechanisms

To understand the role of isolated model mechanisms, we modified the model code to disable the functions responsible for reproducing the vegetation dynamics within in the model (Fig. 5). Unlike the other simulations assessed throughout this paper, the simulation results shown in Fig. 5 begin in the year 1990. i.e. without the use of a spin up period. Removing the spin up period showed that the modified model simulation results produce similar emissions in the first year of the simulation (1990) and allows assessment of the trajectory of deviation.

Disabling the shading scheme (simulation PVN_HEIGHT_CONST) or biomass fraction scheme (simulation PVN_CF_CONST) led to only slightly enhanced $CO_2$ emissions, whereas disabling the FPAR scheme (simulation PVN_FPAR_CONST) led to large $CO_2$ emission differences. Surprisingly, the difference for the PVN_FPAR_CONST simulation is opposite in sign for the two site simulations, and larger for the Ilperveld simulation. This means that maintaining constant FPAR, led to a small

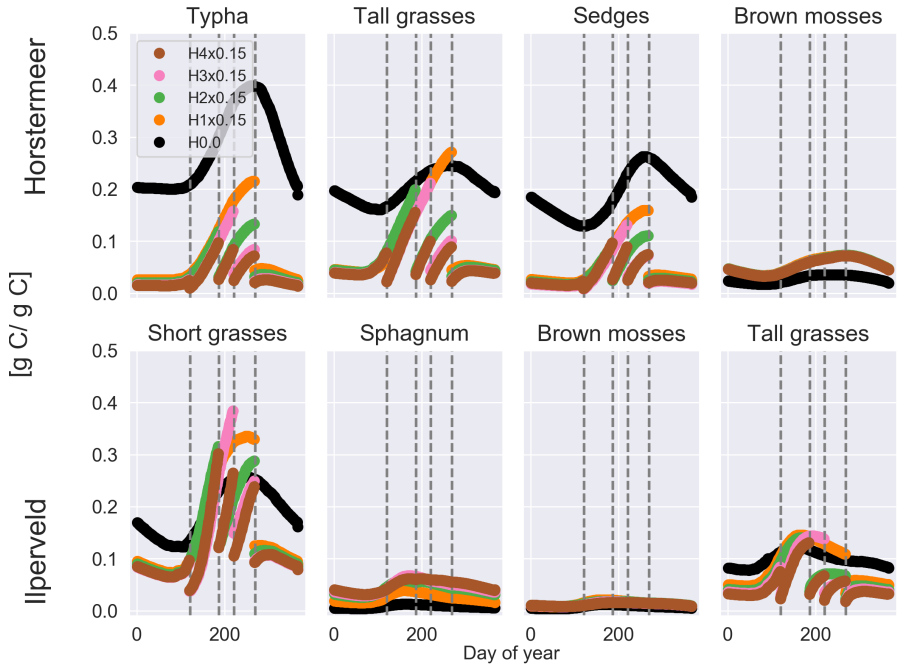


**Figure 4.** The results of the sensitivity tests show the relationship between different harvest schemes and biomass for each day of year (shown as a fraction of litter & root mass) at the Horstermeer site (top row) and Ilperveld site (bottom row). Vegetation is cut to 0.15m (x0.15) at the moment of harvest. The legend shows the harvest input scheme and the vertical dotted lines indicate the four possible harvest days (days 120, 186, 220 and 268). Harvest was set to either not occur (H0.0), occur once per year (H1x0.15) on day 268, twice per year (H2x0.15) on days 186 and 268, three times per year (H3x0.15) on days 120, 220 and 268, or four times per year (H4x0.15) on all harvest days.

enhancement of $CO_2$ fluxes in the Horstermeer simulation but a large reduction of $CO_2$ fluxes for the Ilperveld simulation. These results show that FPAR plays a large role on simulated $CO_2$ emissions. The results of Ilperveld PVN_FPAR_CONST simulation results also showed that the FPAR function has the potential to introduce large variability into the emission results. This is interesting to note because the PVN model showed limited skill reproducing the $CO_2$ emissions at the Ilperveld site. These results indicate that the function calculating FPAR plays a driving role on $CO_2$ emissions but particularly at the Ilperveld site. Further model developments may investigate ways to improve the representation of FPAR in the model. The PVN_FPAR_CONST simulations also led to enhanced $CH_4$ emissions for the Ilperveld simulation. It is likely that $CH_4$ production was enhanced due to increased stores of $CO_2$.

The use of the Peatland-VU $CH_4$ scheme (PVN_CH4_OLD_CF) led to large differences in $CH_4$ emissions for both the Horstermeer and Ilperveld simulations, in comparison to the PVN model results. The $CH_4$ emissions of the model simulations that use the Peatland-VU $CH_4$ scheme (simulation PVN_CH4_OLD_CF) were small when compared to the $CH_4$ emissions of the PVN model, for both model simulations. This indicates that the (PFT) modifications to the $CH_4$ scheme have led to substantial impacts on modeled $CH_4$ emissions.

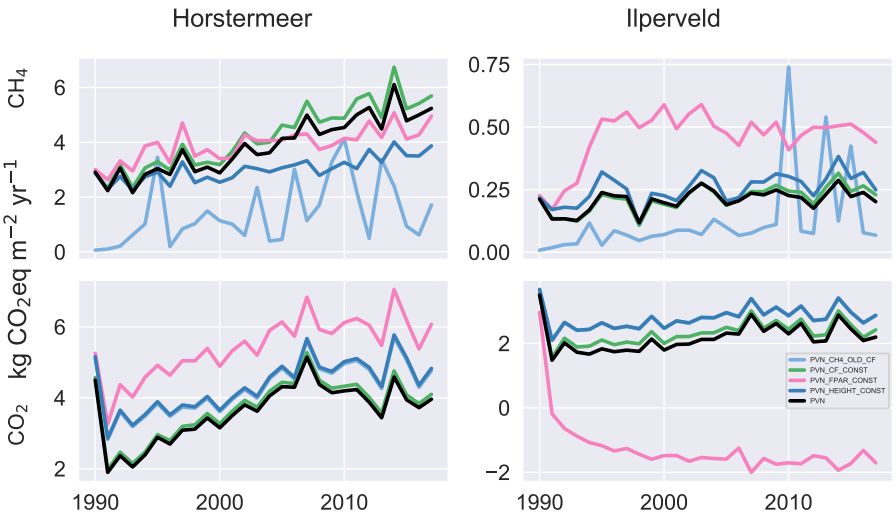


**Figure 5.** The $CH_4$ and $CO_2$ emissions for various isolated model mechanisms, compared against the PVN model result. We investigated maintaining constant fractional PAR (PVN_FPAR_CONST), maintaining constant plant height (PVN_HEIGHT_CONST), maintaining constant cover fraction (PVN_CF_CONST), and including the original Peatland-VU $CH_4$ module multiplied by the PFT cover fraction (PVN_CH4_OLD_CF), at each time step.

### 3.3 Assessment of calibrated model simulations

Here, we describe the simulation results of the model calibrated at two field sites, the Horstermeer and Ilperveld. We describe the net annual $CH_4$ and $CO_2$ emissions, and GHG budgets (Fig. 6), as well as simulated PFT dynamics as indicated by changes to LAI, above-ground biomass, litter mass, and PFT height/depth (Fig. 7 and Fig. S7). All net GHG values are expressed as $CO_2$ equivalents ($CO_{2eq}$) and calculated using 20 (100) year GWPs using equation (31). The model simulation results indicate that the simulated annual mean net GHG emissions from the Ilperveld simulation were approximately half the emissions of the Horstermeer simulation. However, these model emission estimates are not considering off-site decomposition of harvested biomass. The model estimated that the 1995-2017 annual average net GHG emissions were 2.4 (2.3) and 8.0 (5.2) $\mathrm{kgCO_{2eq}m^{-2}yr^{-1}}$ for the Ilperveld and Horstermeer model simulation results, respectively (Fig. 6). The model estimated that the 2015-2017 annual average net GHG emissions were 2.5 (2.3) and 8.9 (5.6) $\mathrm{kgCO_{2eq}m^{-2}yr^{-1}}$ for the Ilperveld and Horstermeer simulations, respectively (Table 6).

Assessment of the Horstermeer simulation showed that on average, $CH_4$ contributed approximately half (52%) of the net annual GHG emissions of the Horstermeer simulation, where $CH_4$ contributed 4.2 $\mathrm{kgCO_{2eq}m^{-2}yr^{-1}}$ and $CO_2$ emissions contributed 3.8 $\mathrm{kgCO_{2eq}m^{-2}yr^{-1}}$, on average. Assessment of the Ilperveld simulation showed that $CO_2$ was the primary contributor to net GHG emissions, where $CO_2$ contributed the majority (92%) of the annual GHG emissions (2.2 $\mathrm{kgCO_{2eq}m^{-2}yr^{-1}}$ of the total 2.4 $\mathrm{kgCO_{2eq}m^{-2}yr^{-1}}$ net GHG emissions). These model emission estimates neglect the off-site decomposition of harvested biomass. Therefore, $CO_2$ and $CH_4$ emissions are equally contributing to the net GHG emissions in the Horstermeer simulation, whereas, $CO_2$ emissions dominate the GHG emissions in the Ilperveld simulation results.

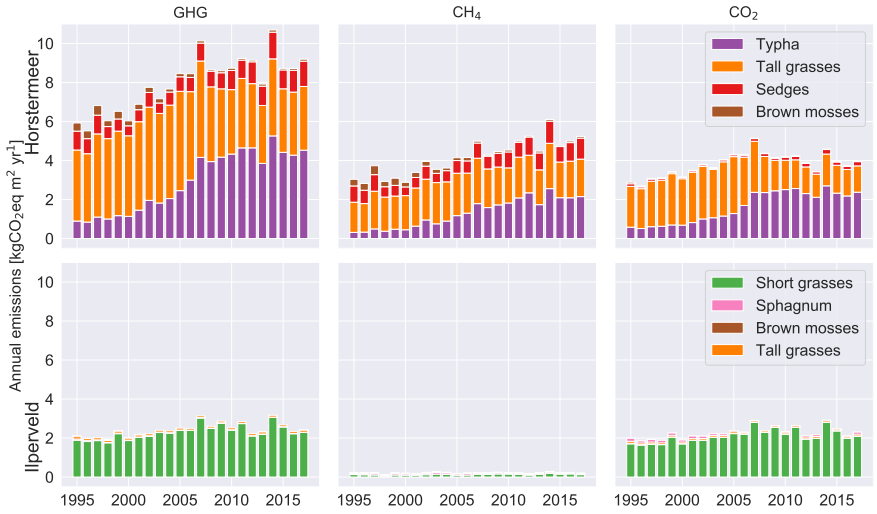


**Figure 6.** Relative contributions of each PFT to simulated annual average net GHG (left), $CH_4$ (middle), and $CO_2$ (right) emissions. The results of the Horstermeer site simulation are represented in the top row and the results of the Ilperveld site simulation are represented in the bottom row.

To assess whether there was an increasing or decreasing trend in emissions over the duration of the simulation (1995-2017), we calculated the linear regression of the $CO_2$, $CH_4$, and net GHG time series of the simulation results at both sites. The trend of Horstermeer simulation emission results was 0.13, 0.06, and 0.19 $\mathrm{kgCO_{2eq}m^{-2}yr^{-1}}$ for $CH_4$, $CO_2$, and the net GHG emissions. Daily temperature observations show local temperatures increased by +0.1C $\mathrm{^{\circ}Cyr^{-1}}$ between 2010 and 2017, or +0.06 $\mathrm{^{\circ}Cyr^{-1}}$ over the entire simulation period (1995-2017). The trend results for the Ilperveld simulation emissions were zero for $CH_4$ emissions, and 0.04 $\mathrm{kgCO_{2eq}m^{-2}yr^{-1}}$ for $CO_2$ and net GHG emissions. Warming temperatures are a possible driver of the enhanced GHG emissions at the Horstermeer site. The increase in GHG emissions of the Horstermeer site simulation and the little or no increase of the Ilperveld site simulation are aligned with the results of the +1$\mathrm{^{\circ}C}$ temperature sensitivity tests. The results of the Horstermeer site sensitivity tests showed that the *Typha* and sedge PFTs were sensitive to warming temperatures, and therefore the increase in the biomass and GHG emissions of the *Typha* and sedge PFTs at the Horstermeer site are likely due to enhanced temperatures.

### 3.3.1 PFT dynamics

Here we describe the living biomass, LAI, litter layer, biomass fraction, and height changes of the PFTs of the calibrated Horstermeer and Ilperveld model simulations (Fig. 7 and Fig. S7). Assessment of above-ground biomass (top row of Fig. 7) shows that the tall grass (blue line), *Typha*, and sedge PFTs (red line), were abundant during the Horstermeer simulation whereas the Ilperveld simulation was dominated by the short grass (green line), *Sphagnum* (pink line) and tall grass PFT (blue line). All plants showed seasonal variability. The ratio of the litter layer to biomass, is between approximately 1:4 and 1:3 for most PFTs (~~kgC~~kg C). The *Typha* PFT is an exception, and the ratio is approximately 1:1. Overall, the sedge PFT

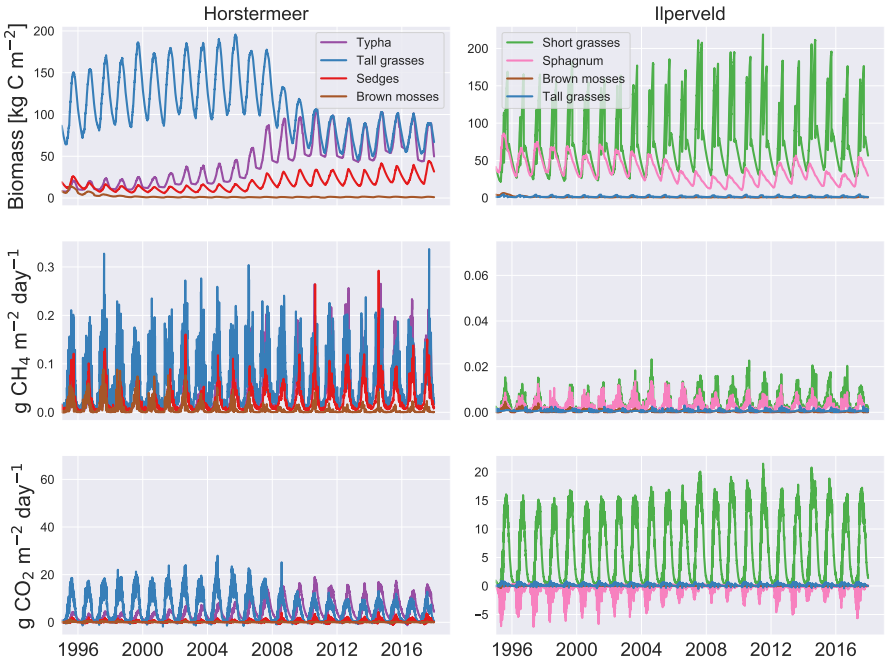


**Figure 7.** Vegetation dynamics. The results of the Horstermeer site simulation are represented in the left column and the results of the Ilperveld site simulation are represented in the right column. Note the differing y axes.

showed comparable seasonal variability to the tall grass PFT whilst maintaining less biomass, smaller LAI, and shorter height throughout the Horstermeer simulation. The similar behaviour of the *Typha*, sedge, and tall grass PFTs ~~were~~ was expected because the PFT input parameters represent similar plant phenologies. Assessment of the size of the litter layer (first row of Fig. S7) showed that in the Ilperveld simulation, the PFTs reached peak litter during Autumn (September) whilst in the Horstermeer simulation which is not mown, the litter continued to accumulate until January where rates of decomposition exceeded accumulation. The LAI (second row of Fig. S7) displayed strong seasonal variability. Each year, the LAI of the Short grasses reaches its maximum LAI value of 1.2. The tall grass PFT, whilst very competitive in the Horstermeer simulation is less competitive in the Ilperveld simulation, partially due to the occurrence of harvests and partially because it is out-competed by the fast growing short grass PFT. Assessment of the Ilperveld simulation reveals that the short grass PFTs were ~~limited by maximum height~~constrained by the maximum height parameter, MaxCanopyHeight. The tall grass PFT was not limited by ~~the maximum height PFT parameter~~ MaxCanopyHeight in the Ilperveld simulation but was instead limited by the biannual mowing regime. PFT height showed strong seasonal variability for both simulations (third row of Fig. S7). The tall grass PFT was the tallest plants in the Horstermeer simulation until 2009 and its height was frequently limited by the PFT ~~maximum height input~~ MaxCanopyHeight parameter. However, as the *Typha* PFT grew in biomass, the tall grass PFT appeared to have less access to sunlight as height and biomass values reduced. The *Typha* and sedge PFTs were not limited by their maximum height parameters. These changes in biomass fraction are also evident in the emissions.

The relative contributions of each PFT towards the and net annual $CH_4$, $CO_2$, and GHG emissions are shown ~~using histogram plots (~~in Fig. 6 ~~)~~ where the $CH_4$ emissions refer to only the plant transported $CH_4$. The net $CO_2$ emissions for each PFT are the sum of the photosynthesis minus respiration, the $CO_2$ produced by belowground aerobic decomposition of ~~inert~~ SOM, and a portion of $CH_4$ oxidised to $CO_2$. The tall grass (red boxes), sedge (orange boxes), and *Typha* (purple boxes) PFTs are large transporters of $CH_4$ emissions of the Horstermeer simulations results. However, only the tall grasses and *Typha* compose the net $CO_2$ emissions in the Horstermeer simulation. Thereby, the tall grass PFT was the largest contributor to the net annual GHG emissions, followed by the *Typha* and sedges PFTs. The Ilperveld simulation results showed that the short grass PFT was the largest contributer to the net annual $CH_4$, $CO_2$, and GHG emissions.

### 3.4 Comparison of modelled and observed plant dynamics

We compare simulated PFT biomass fractions against observed aerial plant cover fractions (Fig. 8). For assessment against observational data we compare model simulation results against observed fluxes by comparing time series, box plots, and 1:1 scatter plots for $CH_4$ (Fig. 9) and $CO_2$ (Fig. 10). Gaps in observational data exist due to measurement collection limitations, and therefore the model comparison against observational data can only be shown for the days where observational data exist. Unfortunately, this means that the model was not assessed equally across all seasons or, on the same days of the year at the two sites. A simple linear regression is used to compare the model simulation results and observational data using all days with available measurements. For these reasons, the 1:1 plots, and $R^2$ linear regression results may only give a flavor of model performance. To understand the degree of uncertainty of the observational measurements, daily standard deviations were derived using the hourly fluxes (plotted as black error bars in Fig. 9 and Fig. 10). In each case the model simulation results generally lay within the spread of observational uncertainty. The observations indicated that both sites are annual sources of $CH_4$ and $CO_2$, and therefore, net annual sources of carbon to the atmosphere. The Horstermeer site (purple line in Fig. 9) and $CO_2$ (Fig. 10) produced large annual mean $CH_4$ and $CO_2$ emissions in comparison to the Ilperveld site (green line in Fig. 9) and $CO_2$ (Fig. 10).

#### 3.4.1 Evaluation of plant composition dynamics

Plant cover fraction observations were made at the location of the chamber measurements and were not representative of the site's plant complete community composition. Although aerial cover fraction and biomass fraction (the ratio of PFT biomass to total biomass) are not the same, changes in plant composition are depicted in both representations.

In 2006, the chamber measurement location at the Hostermeer field site was composed of tall grasses (50%), sedges (40%), *Typha* (5%), and brown mosses (5%) (left panel in Fig. 8). The Horstermeer simulation results have good agreement with the observations but overestimated the amount of tall grasses (66%) and underestimated the amount of Sedges (40%). In 2016, a decade later, the amount of tall grasses remained consistent, whilst the amount of *Typha* had increased by 10%. One year later in 2017, the vegetation had not undergone changes, proportionally. Parallel to the observations, the Horstermeer simulation results estimated that the tall grass PFTs decreased to 60%, from 2005 onwards whilst, the biomass fractions of the *Typha* and sedge PFTs increased. Overall, the Horstermeer simulation overestimated the biomass fraction of the tall grass PFT, and

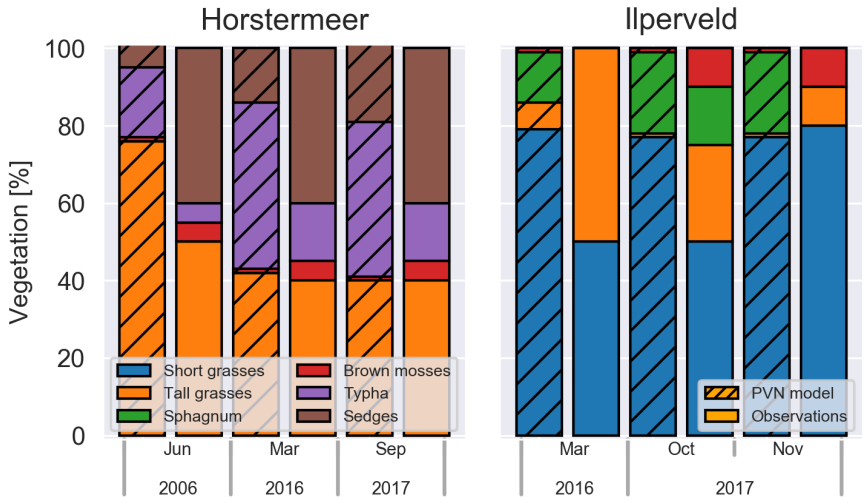


**Figure 8.** Simulated PFT biomass fractions and observed areal cover fractions at Horstermeer (left) and Ilperveld (right).

underestimated the proportion of the sedges and *Typha* PFTs. Model estimates of year-to-year PFT biomass changes were of the same sign and similar magnitude as in situ observations.

In March 2016, the chamber measurement location at the Ilperveld field site hosted short grasses (50%) and tall grasses (50%). The model overestimated the amount of short grasses (80%), underestimated the amount of Tall grasses (5%), and overestimated the amount of *Sphagnum* (10%). The *Omhoog met het Veen* (Raising the Peat) project delivered onsite managements attempts to initiate *Sphagnum* growth by hand dispersing living fragments of *Sphagnum spp.* from a nearby donor site between 2013 and 2015 (Geurts and Fritz, 2018). For this reason, we expected that the model may not match the development of *Sphagnum* at the Ilperveld site. In October 2017, the vegetation shifted to be composed of short grasses (50%), and tall grasses (25%), *Sphagnum* (15%), and brown mosses (10%). One month later in November 2017, the *Sphagnum* was no longer visible (0%), brown mosses remained (10%), and the site was dominated by short grasses (80%). The model estimated that the short grass and *Sphagnum* PFTs remained consistent into 2016 and 2017, whilst the tall grass PFT reduced and brown mosses increased slightly. Whilst the model simulations ended in 2017, we saw that in October 2018, the vegetation remained constant at both sites.

### 3.4.2 Evaluation of simulated $CH_4$ fluxes

The time ~~series1000~~series presented in Fig. 9 shows the behaviour of the Horstermeer simulation $CH_4$ flux results (purple line), the observed mean daily fluxes (black dots) and the spread of the hourly observed fluxes (black error bars). Whilst, the Horstermeer simulation reproduced the seasonal variability of the observed $CH_4$ fluxes, the box plots showed that the simulation results (purple box) tended to overestimate the $CH_4$ fluxes. Overall, the Horstermeer simulation showed a robust pattern of variability when compared with the observations ($R^2 = 0.7$) whilst overestimating the magnitude of observed fluxes.

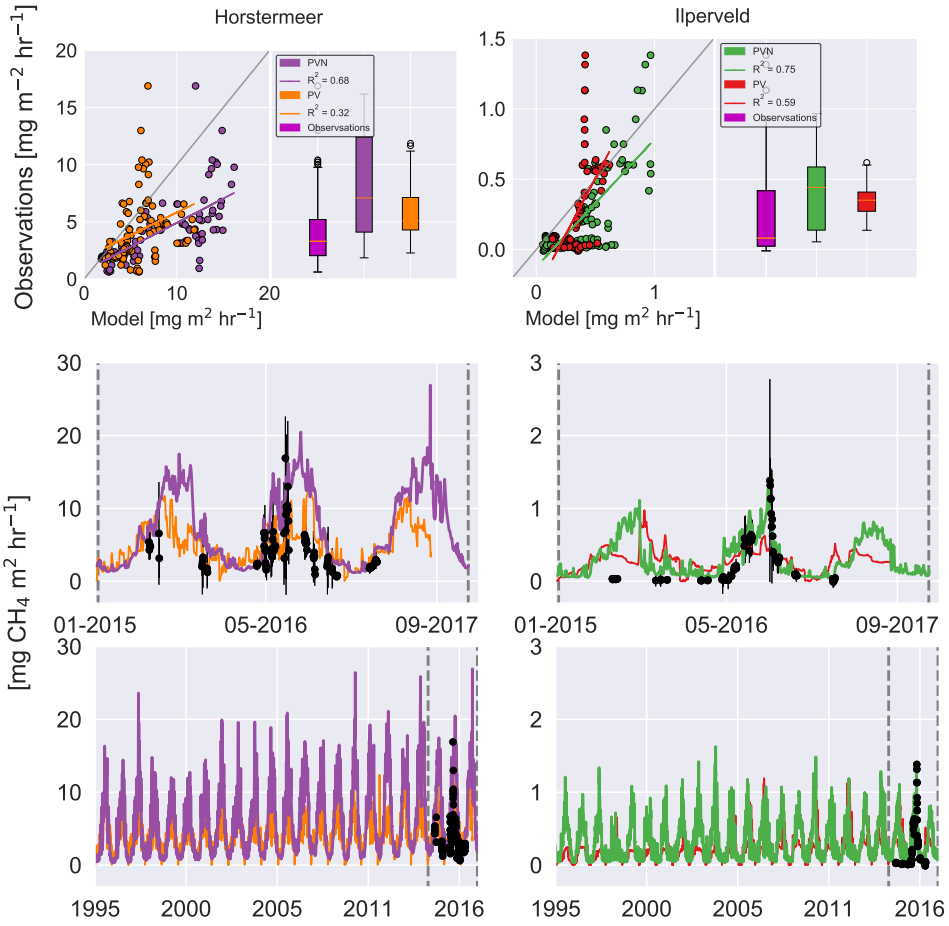


**Figure 9.** Simulated and observed methane fluxes at the Horstermeer (left) and Ilperveld (right). The $R^2$ values are provided for comparison between the new PVN, Peatland-VU model and the observations. In the top panel, the 1:1 line is plotted in grey. The black dots are in situ flux chamber observational measurements in the middle and lower panels. Note the differing x and y axes.

Assessment of the Ilperveld model simulation showed that the model was able to reproduce the observed $CH_4$ fluxes and followed the pattern of variability when compared with the observations ($R^2$ = 0.8). The summer of 2015 is an exception where the simulated results showed an increase in $CH_4$ fluxes, larger than the observed $CH_4$ fluxes. Assessment of the box plots showed that the simulated $CH_4$ fluxes (green box) are of similar mean and spread to the observed fluxes (purple box).

### 3.4.3 Evaluation of simulated $CO_2$ fluxes

The box plots showed that the PVN Horstermeer simulation reproduced the median and range of observed daily $CO_2$ fluxes at the Horstermeer site. The results of the Horstermeer site simulation (purple line) reproduced the 2015, 2016, 2017 Spring $CO_2$ fluxes. The results of the Horstermeer site simulation captured the 2015 and 2016 Autumn fluxes. However, the model generally overestimated the magnitude of simulated fluxes (purple box) but generally reproduced the variability ($R^2$ = 0.8).

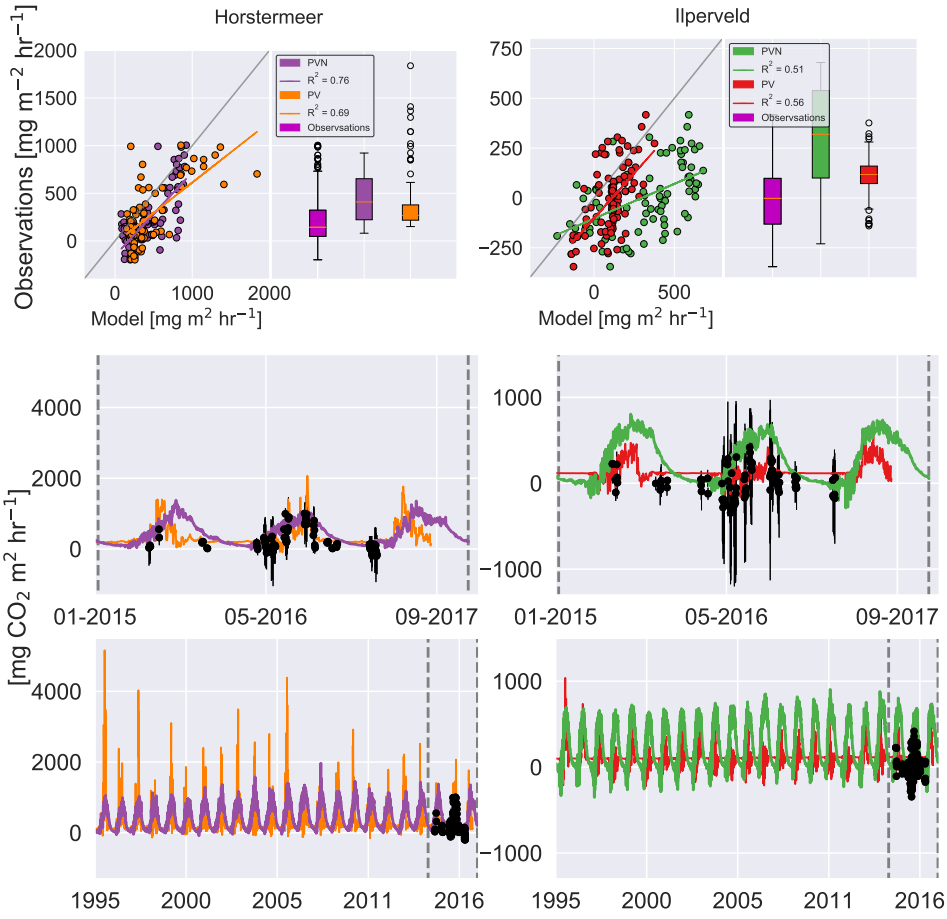


**Figure 10.** Simulated and observed carbon dioxide fluxes (NEE) at the Horstermeer (left) and Ilperveld (right). The $R^2$ values are provided for comparison between the new PVN, Peatland-VU model and the observations. In the top panel, the 1:1 line is plotted in grey. The black dots are in situ flux chamber observational measurements in the middle and lower panels. Note the differing x and y axes.

The box plots in Fig. 10 showed that the Ilperveld simulation results (green box) generally overestimated $CO_2$ fluxes. The box plots showed that the ~~daily~~ mean hourly $CO_2$ flux simulated by the model was a small positive flux, 250mg $\mathrm{mgCO_2m^{-2}hr^{-1}}$ whereas the observed mean hourly flux was 0 $\mathrm{mgCO_2m^{-2}hr^{-1}}$. The Ilperveld simulation (green line) captured the early Spring fluxes in 2016, and 2017. However, during 2015 and 2016, the model tended to overestimate the observed $CO_2$ fluxes. Comparison of the simulated daily hourly average (green line) and the spread of hourly fluxes (black error bars) showed that the simulated $CO_2$ fluxes (green line) fell within the spread of daily hourly fluxes. The model showed some agreement with the observed pattern of variability ($R^2$ = 0.6).

The comparison between the Horstermeer simulation results and observations showed that the model captured the mean daily $CO_2$ fluxes but overestimated $CH_4$ fluxes. The comparison between the Ilperveld simulation results and the observations showed that the model overestimated the mean $CO_2$ fluxes but reproduced the mean and variability of $CH_4$ fluxes.

**Table 6.** Annual average 2015-17 and 1995-2017 $CO_2$, $CH_4$, and GHG emissions. All values are expressed as $CO_2$ equivalents ($kgCO_{2eq}m^{-2}yr^{-1}$) and calculated using 20 (100) year GWP for $CH_4$ and GHG values.

| Site | Model | GHG | | $CO_2$ | | $CH_4$ | |
|---|---|---|---|---|---|---|---|
| | | 2015-17 | 1995-2017 | 2015-17 | 1995-17 | 2015-17 | 1995-17 |
| Horstermeer | PVN | 8.88 (5.56) | 7.96 (5.20) | 3.87 | 3.81 | 5.01 (1.68) | 4.15 (1.40) |
| Horstermeer | PV | 5.90 (3.80) | 5.80 (3.81) | 2.74 | 2.81 | 3.17 (1.07) | 2.99 (1.01) |
| Ilperveld | PVN | 2.47 (2.32) | 2.41 (2.27) | 2.25 | 2.19 | 0.22 (0.08) | 0.22 (0.08) |
| Ilperveld | PV | 1.27 (1.15) | 1.19 (1.08) | 1.09 | 1.03 | 0.18 (0.06) | 0.16 (0.05) |

### 3.5 Comparison to the PEATLAND-VU model

To understand the impact of including vegetation dynamics, we compare the results of the new PVN model against the results of the pre-existing Peatland-VU model (Fig. 9) and $CO_2$ (Fig. 10). The simulation results are summarised in Table 6. Overall, the PVN model estimated the net annual $CH_4$, $CO_2$, and GHG emissions to be larger than the emissions estimates made by the Peatland-VU model. The Peatland-VU model estimated the annual mean 2015-17 GHG emissions to be 1.3 and 5.9 $kgCO_{2eq}m^{-2}yr^{-1}$ for the Ilperveld and Horstermeer simulations, respectively, calculated using a 20yr GWP. When calculated using a 100yr GWP, the Peatland-VU model GHG emission estimates for the Horstermeer simulation were 3.8 $kgCO_{2eq}m^{-2}yr^{-1}$ (for both periods 2015-17 and 1995-2017). The Peatland-VU GHG emission estimates for the Ilperveld simulation were 1.3 and 1.2 $kgCO_{2eq}m^{-2}yr^{-1}$, for the 2015-17 and 1995-2017 periods, respectively.

The comparison of modelled and measured $CH_4$ emissions showed that the PVN model performed well, reproducing $CH_4$ emissions within the spread of observations, in comparison to the Peatland-VU model. The PVN Horstermeer simulation results estimated large mean annual $CH_4$ emissions (5.1 $kgCO_{2eq}m^{-2}yr^{-1}$) in comparison to the Peatland-VU model (3.2 $kgCO_{2eq}m^{-2}yr^{-1}$) for the period 2015-17. The $R^2$ value of the PVN model results in comparison to the observations was 0.7 for the Horstermeer simulation and 0.8 for the Ilperveld simulation. In comparison, the Peatland-VU model results produced $R^2$ values of 0.3 and 0.6 for the Horstermeer and Ilperveld simulations, respectively. The Peatland-VU model showed good skill reproducing the $CO_2$ fluxes at the Horstermeer site ($R^2$ = 0.7) and less skill at the Ilperveld site ($R^2$ = 0.6). Similarly, the PVN model showed good skill reproducing daily $CO_2$ fluxes at the Horstermeer site ($R^2$ = 0.8) but less skill at the Ilperveld site ($R^2$ = 0.6), as indicated by the linear regression results. Overall, assessment of the linear regression results showed that the behaviour of the PVN model performed well against the observations when compared to the Peatland-VU model.

## 4 Discussion

We have developed the PVN model, a new dynamic vegetation-peatland-emissions model capable of understanding the role dynamic PFTs have on $CO_2$ and $CH_4$ emissions in peatlands. ~~The aim of the PVN model is not to outperform the Peatland-VU model but to include representation of dynamic plant processes. For this reason, the model skill may remain comparable to that of the Peatland-VU model.~~ We tested the sensitivity of simulated PFT processes to changing environmental parameters ~~. We~~

have assessed and investigated the impacts of the new schemes introduced into the model that attempt to replicate competition between vegetation types. Here we discuss potential sources of uncertainty, both in the observational data used to evaluate the model results and in the chosen model input parameters. Secondly, we discuss the processes in the model that allow the representation of dynamic vegetation and the ability of these processes to respond to changing environments. Lastly, we discuus discus how the new PVN model compares to its two parent models, the NUCOM-BOG model and the Peatland-VU model, as well as the one other site-specific GHG emissions peatland model that uses dynamic PFTs.

### 4.1 Sources of uncertainty

#### 4.1.1 Input parameters

It is important to note that the Peatland-VU, NUCOM-BOG and PVN are heavily parameter dependent models. The Peatland-VU model has been shown to reproduce observed fluxes using widely different parameter sets which means that the Peatland-VU model has a strong equifinality of parametrisations (van Huissteden et al., 2009) because there is simply not enough data available to constrain all model dynamics. One aim of introducing PFTs into the Peatland-VU model was to develop a model with greater dependence on observational data (measured measurable PFT traits) and less dependence on parameters. Thereby, the model performance against observed fluxes may be similar or only somewhat improved in comparison to what was achieved using the Peatland-VU model but the , reducing the equifinality of the model may be less. It is important that improvements of model processes capture the critical processes, but as simply as possible to minimise problems that arise due to the equifinality of parametrisations (**?**). The introduction of PFTs allowed several Peatland-VU parameters that were previously calibratable to become observation-informed parameters, whilst introducing few new parameters, thereby the net result is a reduction in the breadth of the parameter space.

#### 4.1.2 Site Heterogeneity and chamber measurements

We compare the findings of this study against other studies that have assessed observed $CH_4$ fluxes at the Horstermeer site and discuss uncertainties accompanying the chamber measurement technique. The sites simulated in this study pose challenges because they are degraded peatlands where, easily decomposable carbon is likely to have been mineralised (Dorrepaal et al., 2007; **?**), peat has been artificially removed for centuries (Erkens et al., 2016), and nutrients added during livestock grazing (**?**). It remains unclear what impacts these events continue to have on present day $CO_2$ and $CH_4$ fluxes. Unfortunately, at the time of publication there were no published studies investigating the $CO_2$ or $CH_4$ fluxes measured at the Ilperveld site. The $CH_4$ fluxes observations (0-17 $\mathrm{mgCH_4m^{-2}hr^{-1}}$) presented in this study compared well to reported chamber $CH_4$ fluxes measured at the Horstermeer site from 2003 till 2008 (van Huissteden et al., 2009), in the range of 2-15 $\mathrm{mgCH_4m^{-2}hr^{-1}}$, at an area of the site with a varying water table. Interestingly, the $CH_4$ observations presented measured in a wet area of the Horstermeer site were more than double the measurements measured in dry areas of the Horstermeer between 2004 and 2006, using the manual chamber technique (Hendriks et al., 2007). The different chamber measurement locations used by the two studies may account for some of the observed differences. Heterogeneous vegetation and heterogeneous water levels relative to the surface

are known to impact both automated and manual flux-chamber measurements. For this reason, observational measurements are impacted by the physical placement of flux chambers in the field, leading to potential measurement bias (**??**). At very heterogeneous sites, such as the Horstermeer site, flux strengths vary due to micro-topography (Wania et al., 2010) and chamber measurements have been reported to vary significantly within one site, which may explain differences between studies.

The Horstermeer site has vegetation standing taller than 1m. At times, it was necessary to consider the vegetation height when selecting chamber location to ensure vegetation (even when folded) could fit within measurement chambers. Field measurements that exclude areas covered by tall vegetation may result in a significant underestimation of $CO_2$ or particularly, $CH_4$ fluxes~~where, the~~ . The absence of tall vegetation measurements limits the capacity to ~~model~~ test model representations of tall vegetation processes~~and predict associated~~ , restricting the ability to predict changes in $CO_2$ and $CH_4$ fluxes ~~(?), potentially influencing the and flux estimates~~in the presence of tall vegetation (**?**). Due to the labor-intensive nature of accumulating chamber observations consistently through time, these observational datasets do not offer complete temporal continuity, creating an intermittency bias. The high cost of AC meant that sites could not be measured simultaneously, leading to an interrupted sampling regime that may bias $CO_2$ and $CH_4$ flux estimates (**??**). Most chamber measurements were taken during the plant growing season, assuming that the winter fluxes are negligible which has been shown to not always be the case (**?**). Future studies can benefit from continuous AC measurements.

### 4.1.3 On the efficacy of simulating dynamic vegetation

The PVN model was developed by building upon the functionality and structure of the Peatland-VU model whilst incorporating vegetation dynamics from the NUCOM model. The model has incorporated vegetation dynamics and enhanced the Peatland-VU model's existing carbon cycling processes. Competition is based on water table depth, temperature, vegetation height and shading. To verify that the model dynamics are robust and to understand the sensitivity of the PFTs, we performed model sensitivity simulations.

Considering that the short grass, *Sphagnum* and brown moss PFTs share similar PFT parameters, these three PFTs can respond somewhat similarly. Whilst, the short grass PFT is a non-moss PFT, its parameters are not dissimilar to those of moss PFTs. However, the short grass PFT quickly increases in biomass due to its broad range of temperature and water ~~growth limits~~levels for growth. This means that the short grass PFT provides strong competition against other PFTs. Even though the short grass PFT is height limited, its quickly increasing biomass allows increasing access to PAR, which leads to large amounts of plant respiration, root growth, and net $CO_2$ fluxes when compared to the *Sphagnum* and brown moss PFTs. With only a ~~small~~ shallow root system (maximum 0.1m), moss PFTs have limited abilities to transport below-ground $CO_2$ and as expected, the total below-ground $CO_2$ flux is small for mosses. Whilst, mosses do not have root structures in reality, we allocated moss PFTs to have a presence in the top 10cm of the soil layer because in the presence of bryophytes, there is often no clear separation between the living moss layer and the soil surface. In this way, we intended to replicate a transition zone. Key differences in the parameters between short grasses and brown mosses are that short grasses are not considered a moss PFT (relevant for height growth and light interception)~~, moss (short grass)~~ . In the model, moss PFTs have large ~~(small) MethanePType value, whereas moss PFTs have low LeafRespirationCoeff and BiomassSenescence values~~ $CH_4$vP values, low leaf maintenance respiration

coefficient and biomass senescence values (Table 1). Whilst these differentiations have been somewhat effective, future model versions might consider further ways of distinguishing moss PFTs (especially *Sphagnum*)~~species~~. The presence of *Sphagnum* in SOM increases the acidity of the soil. By influencing the acidity of the soil and limiting the nutrient availability, *Sphagnum* gains an advantage over other plant types because *Sphagnum* flourishes in ~~nutrient poor~~ nutrient-poor conditions (**?**). A useful addition to future model versions may be to adapt the living moss layer to be incorporated into the soil layer, altering the height of the land surface (relative to the water table, for example) and corresponding soil properties (e.g. pH, DBD).

Largely, decomposition of the peat reservoir led to enhanced $CO_2$ fluxes, due to a thick aerobic layer, with low water levels. Modeled photosynthesis and plant respiration are dependent on both temperature and water levels. This enables assessment of the impacts of water availability and extreme temperatures on plant type. Future model applications may consider the relationship between water availability and plant dynamics, and particularly the impacts of drought on both plant photosynthetic capacity, respiration, soil respiration, $CH_4$ production and oxidation.

#### 4.1.4 Impacts of changing temperature input

Studies show that whilst both $CH_4$ production and oxidation rates are enhanced by warming, the net $CH_4$ flux increases with warming because $CH_4$ production increases at a rate faster than oxidation (**?**). As expected, the PVN model simulated enhanced ~~(decreased)~~ $CH_4$ emissions under simulations driven by warmer ~~(cooler )~~ temperatures and simulated reduced $CH_4$ emissions under simulations driven by cooler temperatures. *Sphagnum*, tall grasses, and brown mosses showed unexpected results because they released less $CH_4$ emissions under warmer simulations. This may be indicative of the narrow temperature limits of *Sphagnum* moss. The impacts of temperature on model processes are three-fold. Firstly, the amount of photosynthesis, and plant respiration performed is dependent on the ideal and tolerated PFT growth temperatures. Secondly, the amount of litter converted to below-ground SOM reservoirs is dependent on soil temperatures, where warmer soil temperatures lead to larger amount of litter converted to below-ground reservoirs. Thirdly, decomposition of below-ground SOM is dependent on soil layer temperature (as well as pH, saturation etc.), where soil layers closer to the surface are warmer. Thereby, temperature influences the PFT abundance, size of litter and below-ground SOM reservoirs available for decomposition, and the efficiency of below-ground SOM decomposition in the model. ~~Field~~ The results of our sensitivity analyses are in agreement with field studies which have ~~shown relationships between individual species,~~ found $CH_4$ emissions ~~, and carbon turnover (~~are typically higher when dominated by *Carex*, than ~~*Phragmitis*~~*Eriophorum* ~~, and *Typha* (Günther et al., 2014); *Eriophorum vaginatum*, *Carex rostrata* and *Juncus effusus* (Ström et al., 2005))~~or *Juncus* (Ström et al., 2005; **?**). This is likely partly due to the presence of aerenchyma and partly due to differing litter quality and rates of carbon turnover (**??**).

#### 4.1.5 Belowground decomposition

Enabling different PFTs to contribute to, oxidise, and decompose different below-ground SOM pools, impacted simulated $CO_2$ and $CH_4$ fluxes. Decomposition in the PVN model is dependent on the decomposition rates of different PFTs. Decomposition rates ~~generally follow this order:~~ have been found to differ between forbs, graminoids, deciduous shrubs, and evergreen shrubs (Dorrepaal et al., 2006, 2007, 2009). The ~~peat SOM~~ peat SOM pool of moss PFTs contribute to $CO_2$ and $CH_4$ fluxes because

(*Sphagnum*) mosses are the primary peat-contributing plant and mosses (especially *Sphagnum*) have slow decomposition rates (Hobbie et al., 2000). Moss PFTs are the only PFTs able to contribute to the peat SOM pool which means that the $CH_4$ fluxes arising from decomposition of the peat SOM pool are only transferred to the surface by moss PFTs. Future modelling efforts could work to improve the representation of peat decomposition, whereby $CO_2$ fluxes resulting from the decomposition of peat can be transferred to the surface by both moss and non-moss PFTs. Mosses are prescribed to have maximum 0.1m roots when the model is initialised and remain constant throughout the model simulation. Mosses do not have an above-ground litter layer and instead their living biomass after senescence, is added directly to the below-ground SOM.

#### 4.1.6 ~~Impacts of changing water level input~~Root distribution representation

~~Largely, decomposition of the peat reservoir led to enhanced fluxes, due to a large aerobic layer, with low water levels.~~ Plant transported $CH_4$ and aerobic $CO_2$ production process are dependent on root mass and independent ~~on~~ of above-ground biomass. In the model, the below-ground $CO_2$ flux is comprised of $CO_2$ produced by peat, root exudates, litter, roots, microbial biomass, humic matter, and $CH_4$ oxidation. Root traits play an important role in species competition ~~(Iversen et al., 2015) and use of observational data, such as exudation rates, root mass and shoot mass, would help constrain future versions of the model. Modeled photosynthesis and leaf respiration are independent of water levels because the photosynthesis production model is temperature and not water dependent. Whilst, this may produce representative results in systems that are not water-limited, future model versions may consider the relationship between water availability and plant growth, and particularly the impacts of drought on both plant photosynthetic capacity and respiration.~~ and processes such as leaf:root allocation, turnover, root stocks, and root distributions have been down to be dependent on climate, species, and land cover type (**?**), particularly in Arctic and boreal systems (Iversen et al., 2015). Root distribution is an important structural representation to reliably simulate $CO_2$and $CH_4$fluxes. However, land surface models have, for the most part, used exponential relationships to describe root distribution (**??**). Advances have been made developing knowledge and observational data of root distributions in boreal peatland systems. Whilst, the exponential relationship is representative for several peatland plant types, an alternative root representation to the exponential relationship may be relevant for certain peatland plant types (**?**Iversen et al., 2015). Future model versions may consider introducing alternative root representations.

#### 4.1.7 The impact of harvests on plant competition

The inclusion of harvest has proven necessary to reproduce the seasonal variability of fluxes in grasslands and crops, where crop harvests occur (Van den Hoof et al., 2011). Whilst $CO_2$ emissions were reduced with increased harvest frequency, these emissions are not considering off-site decomposition of harvested biomass. The harvest method implemented in the PVN model was similar to the instantaneous harvest method featured in other dynamic vegetation models (such as JULES, Littleton et al. (2020)), where the plant is reduced to a certain set height and living biomass and LAI are subsequently adjusted accordingly. JULES assumes 100% of lost biomass is harvested whilst killing off a proportion of below- ground biomass that is converted to litter. The PVN model assumes 20% of harvested biomass is lost to litter and does not account for root death. The increased litter layer leads to enhanced emissions resulting from the decomposition of the litter layer. The PFT living biomass is reduced by

the proportional biomass lost, assuming the plant's biomass is uniformly distributed with height, and LAI is recalculated. Root mass observational measurements over time as well as observational data on the impact of harvests on plant productivity would further improve model representations of harvests. Further assessment may investigate in what ways the photosynthesising, and gas conduit capacities of plants are further reduced in the days after harvest and how this can be better captured by the model.

### 4.2 Comparison to other site-specific peatland GHG emission models

Here we compare the functionality of the new PVN model against its parent models; the Peatland-VU and NUCOM-BOG models. We then also compare the functionality of the PVN model against functionality of PEATBOG, the one other site-specific peatland GHG emissions model that includes dynamic vegetation (Table S1).

We have developed a new model capable of understanding the role dynamic PFTs have on $CO_2$ and $CH_4$ emissions in peatlands~~and for this reason, we do not expect the PVN model to outperform the Peatland-VU model but that the model skill should, at least, be comparable to that of the Peatland-VU model~~. The PVN model simulation results estimated the 1995-2017 annually averaged net GHG budget to be larger than the Peatland-VU model, at both sites. We suspect that there are two reasons for this. The first being a trade-off between enhanced $CO_2$ fluxes or enhanced $CH_4$ fluxes. In both the Peatland-VU and PVN models, the $CO_2$ processes are calculated first. Calibration of the photosynthesis and plant respiration related parameters impacts the amount of $CO_2$ available for $CH_4$ production. ~~We found that the production scheme was the~~ Photosynthesis and leaf respiration mechanisms were the greatest cause of uncertainty in the model's ability to reproduce the net GHG budget. Future model versions, may consider ways to constrain the net $CO_2$ flux by improving the response of photosynthesis to environmental variables. To improve upon this in future model versions it may be useful to consider the representation of below-ground carbon decomposition. The below-ground $CH_4$ pool in the Peatland-VU model increased consistently during the model simulation and therefore, an increasing quantity of $CH_4$ was released from the soil profile throughout the simulation, indicating that the fluxes were likely underestimated early in the simulation. The PVN model prescribes each PFT to have root and shoot mass and root depths. This enables each PFT to access different soil layers, and below-ground $CH_4$ and carbon pools, potentially impacting the longterm variability of $CH_4$ emissions. When compared to observed fluxes, the results indicated that the $CO_2$ scheme in the PVN model may have limited skill when applied to peatland sites of certain physical properties. These results cannot be compared with previous modelling studies because the Peatland-VU $CO_2$ production scheme results have not been published since the $CO_2$ production scheme was introduced by **?** for assessment of the impact on simulated $CH_4$ fluxes.

The NUCOM model was developed to assess the impact of climate change on bog ecosystems by analysing simulations lasting 200-500 years. Running the model over time periods similar to the NUCOM's 1760–2000 simulation period, can assess the model's ability to reproduce shifts in vegetation in response to climate variability. This would require model evaluation using multi-centennial observational data, such as macrofossil evidence. To further investigate the impact of climate change on peatland ecosystems future studies may consider using macrofossil data in combination with forward or backward multi-decadal or multi-centennial climate projections.

The PEATBOG model (Wu and Blodau, 2013) is the one other site-specific peatland model that simulates $CO_2$ and $CH_4$ fluxes and includes competition between (moss, shrub, and graminoid) PFTs. The PEATBOG model has simulated the Mer

Bleue Bog in Canada, a pristine (untouched) raised acidic ombrotrophic bog, over a 6 year period. The Mer Bleue Bog is a ~~nutrient poor bog, which is different to~~ nutrient-poor bog, unlike the two sites assessed in this study. The net annual GHG emissions for the Mer Bleue Bog site were small, approximately 0.02% of the GHG emissions observed at the Ilperveld field site in the Netherlands. Peat has been accumulating at this site since 8400 calyrBP and has developed a peat depth of 6m in the center. The PEATBOG model ~~accounts for similar biogeochemical~~ is a complex model that simulates many of the same processes as the PVN model but beyond this also includes representation of the nitrogen cycling, ~~and subsequent~~ electron accepting processes, dissolved inorganic and organic carbon, and subsequent $CO_2$ and $CH_4$ run-off. The PEATBOG model underestimated the annual net GHG emissions (net ecosystem carbon balance), by approximately half of observed field observations. ~~The net annual GHG emissions for the Mer Bleue Bog site were small, approximately 0.02% of the GHG emissions observed at the Ilperveld field site in the Netherlands.~~ Wu and Blodau (2013) noted the sensitivity of the PEATBOG model to temperature, reporting that 1°C of temperature change was enough to initiate a model bias, swaying the model from a source to a sink. This is concurrent with the results of the sensitivity testing performed in this study, which showed that changes in air temperature had large impacts on both $CO_2$ and $CH_4$ emissions. Plot-scale model inter-comparison efforts could help improve the representation of small-scale processes in peatland models. However, the breadth of observational data required to run and test site-specific models, make site specific model inter-comparison efforts cumbersome and difficult.

## 5 Conclusions

Here, we present Peatland-VU-NUCOM v1.0 (PVN), a new site-specific peatland dynamic vegetation emissions model. By including plant-environmental feedbacks, the model can serve wetland management by estimating changes in the GHG balance of peatland sites in response to management decisions or environmental change. The PVN model was designed to simulate plant competition above and below-ground, whilst developing carbon pools for the production and oxidation of $CH_4$ and $CO_2$. Peatlands are one of the most important carbon storing ecosystems. The challenges facing our understanding of the carbon balance and $CH_4$ dynamics subsequent to the rewetting of previously managed peatlands are numerous. One challenge is the ability of site-specific peatland models to reproduce methane fluxes, particularly in relation to plant functioning. This question is particularly timely because there exists an urgent need to restore drained peatlands to reduce land subsidence whilst limiting GHG emissions. ~~Here, we present Peatland-VU-NUCOM v1.0 (PVN), a new site-specific peatland dynamic vegetation emissions model. PVN was designed to simulate plant competition above and below-ground, whilst developing carbon pools for the production and oxidation of and .~~ We showed that the PVN model was able to reproduce plant biomass fractions, $CH_4$ and $CO_2$ fluxes. This confirms that the model provides the capability to understand the relationship between peatland plant dynamics, $CH_4$ and $CO_2$ emissions. The PVN model is a relevant tool that can be used to optimize vegetation management with the goal to reduce GHG emissions.

*Code and data availability.* All model code has been written in C++. The model code is publicly available from the Bitbucket repository (bitbucket.org/tlippmann/pvn_public, last accessed 30 May 2023) under the GNU General Public License version 3, or any later version. Users are welcome to contact the authors for technical support. All input data used to generate the model simulations presented in this study can be accessed through this Bitbucket. This includes site model parameterisations, site soil profiles, climate data, water level data, and PFTs. The exact version of the model source code used to produce the results presented in this paper is archived on Zenodo (https://zenodo.org/record/8065235, **?**).

*Author contributions.* TL, KvH, and MH developed the theoretical framework of the model. TL performed the model developments, composed the PFTs, made the figures, all analyses, and wrote the paper. TL and KvH collected the observational data, developed the model parameterisation scheme, and soil profiles. KvH processed the observational data and offered valuable suggestions on the development and calibration of the model. YvdV offered valuable suggestions on the testing of the model, the presentation of analyses, and the writing of the manuscript. HD participated in the writing of this paper. HD, MH, KvH,YvdV participated in the revision of this paper. DH, HD, MH, and KvH acquired the funding and administered this project.

*Competing interests.* The contact author has declared that neither they nor their co-authors have any competing interests.

*Acknowledgements.* We would like to thank the editor and the reviewers for their valuable comments and suggestions. We ~~thank~~ acknowledge Merit van den Berg for ~~proof-reading~~valuable discussions regarding peatland processes and Sander Veraverbeke for valuable discussions surrounding the model.

## References


Abdalla, M., Hastings, A., Truu, J., Espenberg, M., Mander, U., and Smith, P.: Emissions of methane from northern peatlands: a review of management impacts and implications for future management options, Ecology and Evolution, 6, 7080–7102, https://doi.org/10.1002/ece3.2469, 2016.

Alhoz, K., Kenesei, K., Papageorgiou, M., Keurentjes, E. E. M., and de Jong, M.: Improved AHN3 Gridded DTM/DSM, 2020.

Baldocchi, D. D.: Assessing the eddy covariance technique for evaluating carbon dioxide exchange rates of ecosystems: Past, present and future, Global Change Biology, 9, 479–492, https://doi.org/10.1046/j.1365-2486.2003.00629.x, 2003.

Baldocchi, D. D. and Harley, P. C.: Scaling carbon dioxide and water vapour exchange from leaf to canopy in a deciduous forest. II. Model testing and application, Plant, Cell and Environment, 18, 1157–1173, https://doi.org/10.1111/j.1365-3040.1995.tb00626.x, 1995.

Ballantyne, D. M., Hribljan, J. A., Pypker, T. G., and Chimner, R. A.: Long-term water table manipulations alter peatland gaseous carbon fluxes in Northern Michigan, Wetlands Ecology and Management, 22, 35–47, https://doi.org/10.1007/s11273-013-9320-8, 2014.

Bao, T., Jia, G., and Xu, X.: Weakening greenhouse gas sink of pristine wetlands under warming, Nature Climate Change, 13, https://doi.org/10.1038/s41558-023-01637-0, 2023.

Basile-Doelsch, I., Balesdent, J., and Pellerin, S.: Reviews and syntheses: The mechanisms underlying carbon storage in soil, Biogeosciences, 17, 5223–5242, https://doi.org/10.5194/bg-17-5223-2020, 2020.

Beven, K. and Freer, J.: Equifinality, data assimilation, and uncertainty estimation in mechanistic modelling of complex environmental systems using the GLUE methodology, Journal of Hydrology, 249, 11–29, https://doi.org/10.1016/S0022-1694(01)00421-8, 2001.

Boonman, J., Hefting, M. M., Van Huissteden, C. J., Van Den Berg, M., Van Huissteden, J., Erkens, G., Melman, R., and Van Der Velde, Y.: Cutting peatland CO2 emissions with water management practices, Biogeosciences, 19, 5707–5727, https://doi.org/10.5194/bg-19-5707-2022, https://doi.org/10.5194/bg-19-5707-2022, 2022.

Box, J. E., Colgan, W. T., Christensen, T. R., Schmidt, N. M., Lund, M., Parmentier, F. J. W., Brown, R., Bhatt, U. S., Euskirchen, E. S., Romanovsky, V. E., Walsh, J. E., Overland, J. E., Wang, M., Corell, R. W., Meier, W. N., Wouters, B., Mernild, S., Mård, J., Pawlak, J., and Olsen, M. S.: Key indicators of Arctic climate change: 1971-2017, Environmental Research Letters, 14, https://doi.org/10.1088/1748-9326/aafc1b, 2019.

Bridgham, S. D., Cadillo-Quiroz, H., Keller, J. K., and Zhuang, Q.: Methane emissions from wetlands: Biogeochemical, microbial, and modeling perspectives from local to global scales, Global Change Biology, 19, 1325–1346, https://doi.org/10.1111/gcb.12131, 2013.

Bubier, J. L.: The Relationship of Vegetation to Methane Emission and Hydrochemical Gradients in Northern Peatlands, Journal of Ecology, 83, 403–420, http://www.jstor.org/stable/2261594, 2016.

Chaney, N. W., Sheffield, J., Villarini, G., and Wood, E. F.: Development of a high-resolution gridded daily meteorological dataset over sub-Saharan Africa: Spatial analysis of trends in climate extremes, Journal of Climate, 27, 5815–5835, https://doi.org/10.1175/JCLI-D-13-00423.1, 2014.

Christensen, T. R., Ekberg, A., Ström, L., Mastepanov, M., Panikov, N., Öquist, M., Svensson, B. H., Nykänen, H., Martikainen, P. J., and Oskarsson, H.: Factors controlling large scale variations in methane emissions from wetlands, Geophysical Research Letters, 30, 1–4, https://doi.org/10.1029/2002GL016848, 2003.

Churkina, G., Running, S. W., and Schloss, A. L.: Comparing global models of terrestrial net primary productivity (NPP): The importance of water availability, Global Change Biology, 5, 46–55, https://doi.org/10.1046/j.1365-2486.1999.00006.x, 1999.

Clemmensen, K. E., Bahr, A., Ovaskainen, O., Dahlberg, A., Ekblad, A., Wallander, H., Stenlid, J., Finlay, R. D., Wardle, D. A., and Lindahl, B. D.: Roots and Associated Fungi Drive Long-Term Carbon Sequestration in Boreal Forest, Science, 339, 1615–1618, https://doi.org/10.1126/science.1231923, https://www.sciencemag.org/lookup/doi/10.1126/science.1231923, 2013.

Crow, S. E. and Wieder, R. K.: Sources of CO2 emission from a northern peatland: Root respiration, exudation, and decomposition, Ecology, 86, 1825–1834, https://doi.org/10.1890/04-1575, 2005.

Davidson, E. and Janssens, I. A.: Temperature sensitivity of soil carbon decomposition and feedbacks to climate change., Nature, 440, 165–173, https://doi.org/10.1038/nature04514, 2006a.

Davidson, E. A. and Janssens, I. A.: Temperature sensitivity of soil carbon decomposition and feedbacks to climate change, Nature, 440, 165–173, https://doi.org/10.1038/nature04514, 2006b.

De Boeck, H. J., Dreesen, F. E., Janssens, I. A., and Nijs, I.: Whole-system responses of experimental plant communities to climate extremes imposed in different seasons, New Phytologist, 189, 806–817, https://doi.org/10.1111/j.1469-8137.2010.03515.x, http://www.ncbi.nlm.nih.gov/pubmed/21054412, 2011.

De La Motte, L. G., Beauclaire, Q., Heinesch, B., Cuntz, M., Foltýnová, L., Šigut, L., Kowalska, N., Manca, G., Ballarin, I. G., Vincke, C., Roland, M., Ibrom, A., Lousteau, D., Siebicke, L., Neiryink, J., and Longdoz, B.: Non-stomatal processes reduce gross primary productivity in temperate forest ecosystems during severe edaphic drought: Edaphic drought in forest ecosystems, Philosophical Transactions of the Royal Society B: Biological Sciences, 375, https://doi.org/10.1098/rstb.2019.0527, 2020.

De Lange, W. J., Prinsen, G. F., Hoogewoud, J. C., Veldhuizen, A. A., Verkaik, J., Oude Essink, G. H., Van Walsum, P. E., Delsman, J. R., Hunink, J. C., Massop, H. T. L., and Kroon, T.: An operational, multi-scale, multi-model system for consensus-based, integrated water management and policy analysis: The Netherlands Hydrological Instrument., Environmental Modelling and Software, 59, 98–108, https://doi.org/10.1016/j.envsoft.2014.05.009, http://dx.doi.org/10.1016/j.envsoft.2014.05.009, 2014.

Dick, J. J., Tetzlaff, D., Birkel, C., and Soulsby, C.: Modelling landscape controls on dissolved organic carbon sources and fluxes to streams, Biogeochemistry, 122, 361–374, https://doi.org/10.1007/s10533-014-0046-3, http://link.springer.com/10.1007/s10533-014-0046-3, 2015.

Dorrepaal, E., Aerts, R., Cornelissen, J. H., Van Logtestijn, R. S., and Callaghan, T. V.: Sphagnum modifies climate-change impacts on subarctic vascular bog plants, Functional Ecology, 20, 31–41, https://doi.org/10.1111/j.1365-2435.2006.01076.x, 2006.

Dorrepaal, E., Cornelissen, J. H., and Aerts, R.: Changing leaf litter feedbacks on plant production across contrasting sub-arctic peatland species and growth forms, Oecologia, 151, 251–261, https://doi.org/10.1007/s00442-006-0580-3, 2007.

Dorrepaal, E., Toet, S., Van Logtestijn, R. S., Swart, E., Van De Weg, M. J., Callaghan, T. V., and Aerts, R.: Carbon respiration from subsurface peat accelerated by climate warming in the subarctic, Nature, 460, 616–619, https://doi.org/10.1038/nature08216, http://dx.doi.org/10.1038/nature08216, 2009.

Erkens, G., Van Der Meulen, M. J., and Middelkoop, H.: Double trouble: Subsidence and CO2 respiration due to 1,000 years of Dutch coastal peatlands cultivation, Hydrogeology Journal, 24, 551–568, https://doi.org/10.1007/s10040-016-1380-4, 2016.

Evans, C. D., Peacock, M., Baird, A. J., Artz, R. R., Burden, A., Callaghan, N., Chapman, P. J., Cooper, H. M., Coyle, M., Craig, E., Cumming, A., Dixon, S., Gauci, V., Grayson, R. P., Helfter, C., Heppell, C. M., Holden, J., Jones, D. L., Kaduk, J., Levy, P., Matthews, R., McNamara, N. P., Misselbrook, T., Oakley, S., Page, S. E., Rayment, M., Ridley, L. M., Stanley, K. M., Williamson, J. L., Worrall, F., and Morrison, R.: Overriding water table control on managed peatland greenhouse gas emissions, Nature, 593, 548–552, https://doi.org/10.1038/s41586-021-03523-1, http://dx.doi.org/10.1038/s41586-021-03523-1, 2021.

Frolking, S. and Roulet, N. T.: Holocene radiative forcing impact of northern peatland carbon accumulation and methane emissions, Global Change Biology, 13, 1079–1088, https://doi.org/10.1111/j.1365-2486.2007.01339.x, 2007.

Geurts, J. and Fritz, C.: Paludiculture pilots and experiments with focus on cattail and reed in the Netherlands. Technical, Tech. rep., Radboud University Nijmegen, Nijmegen, https://repository.ubn.ru.nl/handle/2066/192628, 2018.

Gorham, E.: Shoot height, weight and standing crop in relation to density of monospecific plant stands, Nature, 279, 148–150, https://doi.org/10.1038/279148a0, https://www.nature.com/articles/279148a0, 1979.

Graf, M. and Rochefort, L.: Examining the peat-accumulating potential of fen vegetation in the context of fen restoration of harvested peatlands, Ecoscience, 16, 158–166, https://doi.org/10.2980/16-2-3128, 2009.

Granberg, G., Grip, H., Ottosson Löfvenius, M., Sundh, I., Svensson, B. H., and Nilsson, M.: A simple model for simulation of water content, soil frost, and soil temperatures in boreal mixed mires, Water Resources Research, 35, 3771–3782, https://doi.org/10.1029/1999WR900216, 1999.

Günther, A., Huth, V., Jurasinski, G., and Glatzel, S.: The effect of biomass harvesting on greenhouse gas emissions from a rewetted temperate fen, GCB Bioenergy, 7, 1092–1106, https://doi.org/10.1111/gcbb.12214, 2015.

Günther, A., Barthelmes, A., Huth, V., Joosten, H., Jurasinski, G., Koebsch, F., and Couwenberg, J.: Prompt rewetting of drained peatlands reduces climate warming despite methane emissions, Nature Communications, 11, 1644, https://doi.org/10.1038/s41467-020-15499-z, http://www.nature.com/articles/s41467-020-15499-z, 2020.

Gupta, H. V., Kling, H., Yilmaz, K. K., and Martinez, G. F.: Decomposition of the mean squared error and NSE performance criteria: Implications for improving hydrological modelling, Journal of Hydrology, 377, 80–91, https://doi.org/10.1016/j.jhydrol.2009.08.003, http://dx.doi.org/10.1016/j.jhydrol.2009.08.003, 2009.

Harpenslager, S. F., van den Elzen, E., Kox, M. A., Smolders, A. J., Ettwig, K. F., and Lamers, L. P.: Rewetting former agricultural peatlands: Topsoil removal as a prerequisite to avoid strong nutrient and greenhouse gas emissions, Ecological Engineering, 84, 159–168, https://doi.org/10.1016/j.ecoleng.2015.08.002, http://dx.doi.org/10.1016/j.ecoleng.2015.08.002, 2015.

Haxeltine, A. and Prentice, I. C.: BIOME3: An equilibrium terrestrial biosphere model based on ecophysiological constraints, resource availability, and competition among plant functional types, Global Biogeochemical Cycles, 10, 693–709, https://doi.org/10.1029/96GB02344, http://doi.wiley.com/10.1029/96GB02344, 1996a.

Haxeltine, A. and Prentice, I. C.: A General Model for the Light-Use Efficiency of Primary Production, Functional Ecology, 10, 551, https://doi.org/10.2307/2390165, https://www.jstor.org/stable/2390165?origin=crossref, 1996b.

Heijmans, M. and Berendse, F.: NUCOM: a dynamic vegetation model for peatlands and tundra including nitrogen cycling and mosses, 2008.

Heijmans, M. M., Mauquoy, D., Van Geel, B., and Berendse, F.: Long-term effects of climate change on vegetation and carbon dynamics in peat bogs, Journal of Vegetation Science, 19, 307–320, https://doi.org/10.3170/2008-8-18368, https://www.scopus.com/inward/record.url?eid=2-s2.0-41849115693&partnerID=40&md5=650f510b7f8fb783728dc3e00073b873, 2008.

Hendriks, D. M., Van Huissteden, J., Dolman, A. J., and Van Der Molen, M. K.: The full greenhouse gas balance of an abandoned peat meadow, Biogeosciences, 4, 411–424, https://doi.org/10.5194/bg-4-411-2007, 2007.

Hobbie, S. E., Schimel, J. P., Trumbore, S. E., and Randerson, J. R.: Controls over carbon storage and turnover in high-latitude soils, Global Change Biology, 6, 196–210, https://doi.org/10.1046/j.1365-2486.2000.06021.x, 2000.

Högberg, P., Nordgren, A., Buchmann, N., Taylor, A. F., Ekblad, A., Högberg, M. N., Nyberg, G., Ottosson-Löfvenius, M., and Read, D. J.: Large-scale forest girdling shows that current photosynthesis drives soil respiration, Nature, 411, 789–792, https://doi.org/10.1038/35081058, 2001.

Huang, S., Titus, S. J., and Wiens, D. P.: Comparison of nonlinear height-diameter functions for major Alberta tree species, Canadian Journal of Forest Research, 22, 1297–1304, https://doi.org/10.1139/x92-172, https://cdnsciencepub.com/doi/10.1139/x92-172http://www.nrcresearchpress.com/doi/10.1139/x92-172, 1992.

Iversen, C. M., Sloan, V. L., Sullivan, P. F., Euskirchen, E. S., Mcguire, A. D., Norby, R. J., Walker, A. P., Warren, J. M., and Wullschleger, S. D.: The unseen iceberg: Plant roots in arctic tundra, New Phytologist, 205, 34–58, https://doi.org/10.1111/nph.13003, http://www.ncbi.nlm.nih.gov/pubmed/25209220https://onlinelibrary.wiley.com/doi/10.1111/nph.13003, 2015.

Jaatinen, K., Laiho, R., Vuorenmaa, A., Del Castillo, U., Minkkinen, K., Pennanen, T., Penttilä, T., and Fritze, H.: Responses of aerobic microbial communities and soil respiration to water-level drawdown in a northern boreal fen, Environmental Microbiology, 10, 339–353, https://doi.org/10.1111/j.1462-2920.2007.01455.x, 2008.

Jackowicz-Korczyński, M., Christensen, T. R., Bäckstrand, K., Crill, P., Friborg, T., Mastepanov, M., and Ström, L.: Annual cycle of methane emission from a subarctic peatland, Journal of Geophysical Research: Biogeosciences, 115, 1–10, https://doi.org/10.1029/2008JG000913, 2010.

Jackson, R. B., Canadell, J., Ehleringer, J. R., Mooney, H. A., Sala, O. E., and Schulze, E. D.: A global analysis of root distributions for terrestrial biomes, Oecologia, 108, 389–411, https://doi.org/10.1007/BF00333714, 1996.

Järveoja, J., Laht, J., Maddison, M., Soosaar, K., Ostonen, I., and Mander, Ü.: Mitigation of greenhouse gas emissions from an abandoned Baltic peat extraction area by growing reed canary grass: Life-cycle assessment, Regional Environmental Change, 13, 781–795, https://doi.org/10.1007/s10113-012-0355-9, 2013.

Kattge, J., Díaz, S., Lavorel, S., Prentice, I. C., Leadley, P., Bönisch, G., Garnier, E., Westoby, M., Reich, P. B., Wright, I. J., Cornelissen, J. H., Violle, C., Harrison, S. P., Van Bodegom, P. M., Reichstein, M., Enquist, B. J., Soudzilovskaia, N. A., Ackerly, D. D., Anand, M., Atkin, O., Bahn, M., Baker, T. R., Baldocchi, D., Bekker, R., Blanco, C. C., Blonder, B., Bond, W. J., Bradstock, R., Bunker, D. E., Casanoves, F., Cavender-Bares, J., Chambers, J. Q., Chapin, F. S., Chave, J., Coomes, D., Cornwell, W. K., Craine, J. M., Dobrin, B. H., Duarte, L., Durka, W., Elser, J., Esser, G., Estiarte, M., Fagan, W. F., Fang, J., Fernández-Méndez, F., Fidelis, A., Finegan, B., Flores, O., Ford, H., Frank, D., Freschet, G. T., Fyllas, N. M., Gallagher, R. V., Green, W. A., Gutierrez, A. G., Hickler, T., Higgins, S. I., Hodgson, J. G., Jalili, A., Jansen, S., Joly, C. A., Kerkhoff, A. J., Kirkup, D., Kitajima, K., Kleyer, M., Klotz, S., Knops, J. M., Kramer, K., Kühn, I., Kurokawa, H., Laughlin, D., Lee, T. D., Leishman, M., Lens, F., Lenz, T., Lewis, S. L., Lloyd, J., Llusià, J., Louault, F., Ma, S., Mahecha, M. D., Manning, P., Massad, T., Medlyn, B. E., Messier, J., Moles, A. T., Müller, S. C., Nadrowski, K., Naeem, S., Niinemets, Ü., Nöllert, S., Nüske, A., Ogaya, R., Oleksyn, J., Onipchenko, V. G., Onoda, Y., Ordoñez, J., Overbeck, G., Ozinga, W. A., Patiño, S., Paula, S., Pausas, J. G., Peñuelas, J., Phillips, O. L., Pillar, V., Poorter, H., Poorter, L., Poschlod, P., Prinzing, A., Proulx, R., Rammig, A., Reinsch, S., Reu, B., Sack, L., Salgado-Negret, B., Sardans, J., Shiodera, S., Shipley, B., Siefert, A., Sosinski, E., Soussana, J. F., Swaine, E., Swenson, N., Thompson, K., Thornton, P., Waldram, M., Weiher, E., White, M., White, S., Wright, S. J., Yguel, B., Zaehle, S., Zanne, A. E., and Wirth, C.: TRY - a global database of plant traits, Global Change Biology, 17, 2905–2935, https://doi.org/10.1111/j.1365-2486.2011.02451.x, 2011.

Kattge, J., Bönisch, G., Díaz, S., Lavorel, S., Prentice, I. C., Leadley, P., Tautenhahn, S., Werner, G. D., Aakala, T., Abedi, M., Acosta, A. T., Adamidis, G. C., Adamson, K., Aiba, M., Albert, C. H., Alcántara, J. M., Alcázar C, C., Aleixo, I., Ali, H., Amiaud, B., Ammer, C., Amoroso, M. M., Anand, M., Anderson, C., Anten, N., Antos, J., Apgaua, D. M. G., Ashman, T. L., Asmara, D. H., Asner, G. P., Aspinwall, M., Atkin, O., Aubin, I., Baastrup-Spohr, L., Bahalkeh, K., Bahn, M., Baker, T., Baker, W. J., Bakker, J. P., Baldocchi, D., Baltzer, J., Banerjee, A., Baranger, A., Barlow, J., Barneche, D. R., Baruch, Z., Bastianelli, D., Battles, J., Bauerle, W., Bauters, M., Bazzato, E., Beckmann, M., Beeckman, H., Beierkuhnlein, C., Bekker, R., Belfry, G., Belluau, M., Beloiu, M., Benavides, R., Benomar,

L., Berdugo-Lattke, M. L., Berenguer, E., Bergamin, R., Bergmann, J., Bergmann Carlucci, M., Berner, L., Bernhardt-Römermann, M., Bigler, C., Bjorkman, A. D., Blackman, C., Blanco, C., Blonder, B., Blumenthal, D., Bocanegra-González, K. T., Boeckx, P., Bohlman, S., Böhning-Gaese, K., Boisvert-Marsh, L., Bond, W., Bond-Lamberty, B., Boom, A., Boonman, C. C., Bordin, K., Boughton, E. H., Boukili, V., Bowman, D. M., Bravo, S., Brendel, M. R., Broadley, M. R., Brown, K. A., Bruelheide, H., Brumnich, F., Bruun, H. H., Bruy, D., Buchanan, S. W., Bucher, S. F., Buchmann, N., Buitenwerf, R., Bunker, D. E., Bürger, J., Burrascano, S., Burslem, D. F., Butterfield, B. J., Byun, C., Marques, M., Scalon, M. C., Caccianiga, M., Cadotte, M., Cailleret, M., Camac, J., Camarero, J. J., Campany, C., Campetella, G., Campos, J. A., Cano-Arboleda, L., Canullo, R., Carbognani, M., Carvalho, F., Casanoves, F., Castagneyrol, B., Catford, J. A., Cavender-Bares, J., Cerabolini, B. E., Cervellini, M., Chacón-Madrigal, E., Chapin, K., Chapin, F. S., Chelli, S., Chen, S. C., Chen, A., Cherubini, P., Chianucci, F., Choat, B., Chung, K. S., Chytrý, M., Ciccarelli, D., Coll, L., Collins, C. G., Conti, L., Coomes, D., Cornelissen, J. H., Cornwell, W. K., Corona, P., Coyea, M., Craine, J., Craven, D., Cromsigt, J. P., Csecserits, A., Cufar, K., Cuntz, M., da Silva, A. C., Dahlin, K. M., Dainese, M., Dalke, I., Dalle Fratte, M., Dang-Le, A. T., Danihelka, J., Dannoura, M., Dawson, S., de Beer, A. J., De Frutos, A., De Long, J. R., Dechant, B., Delagrange, S., Delpierre, N., Derroire, G., Dias, A. S., Diaz-Toribio, M. H., Dimitrakopoulos, P. G., Dobrowolski, M., Doktor, D., Dřevojan, P., Dong, N., Dransfield, J., Dressler, S., Duarte, L., Ducouret, E., Dullinger, S., Durka, W., Duursma, R., Dymova, O., E-Vojtkó, A., Eckstein, R. L., Ejtehadi, H., Elser, J., Emilio, T., Engemann, K., Erfanian, M. B., Erfmeier, A., Esquivel-Muelbert, A., Esser, G., Estiarte, M., Domingues, T. F., Fagan, W. F., Fagúndez, J., Falster, D. S., Fan, Y., Fang, J., Farris, E., Fazlioglu, F., Feng, Y., Fernandez-Mendez, F., Ferrara, C., Ferreira, J., Fidelis, A., Finegan, B., Firn, J., Flowers, T. J., Flynn, D. F., Fontana, V., Forey, E., Forgiarini, C., François, L., Frangipani, M., Frank, D., Frenette-Dussault, C., Freschet, G. T., Fry, E. L., Fyllas, N. M., Mazzochini, G. G., Gachet, S., Gallagher, R., Ganade, G., Ganga, F., García-Palacios, P., Gargaglione, V., Garnier, E., Garrido, J. L., de Gasper, A. L., Gea-Izquierdo, G., Gibson, D., Gillison, A. N., Giroldo, A., Glasenhardt, M. C., Gleason, S., Gliesch, M., Goldberg, E., Göldel, B., Gonzalez-Akre, E., Gonzalez-Andujar, J. L., González-Melo, A., González-Robles, A., Graae, B. J., Granda, E., Graves, S., Green, W. A., Gregor, T., Gross, N., Guerin, G. R., Günther, A., Gutiérrez, A. G., Haddock, L., Haines, A., Hall, J., Hambuckers, A., Han, W., Harrison, S. P., Hattingh, W., Hawes, J. E., He, T., He, P., Heberling, J. M., Helm, A., Hempel, S., Hentschel, J., Hérault, B., Hereş, A. M., Herz, K., Heuertz, M., Hickler, T., Hietz, P., Higuchi, P., Hipp, A. L., Hirons, A., Hock, M., Hogan, J. A., Holl, K., Honnay, O., Hornstein, D., Hou, E., Hough-Snee, N., Hovstad, K. A., Ichie, T., Igić, B., Illa, E., Isaac, M., Ishihara, M., Ivanov, L., Ivanova, L., Iversen, C. M., Izquierdo, J., Jackson, R. B., Jackson, B., Jactel, H., Jagodzinski, A. M., Jandt, U., Jansen, S., Jenkins, T., Jentsch, A., Jespersen, J. R. P., Jiang, G. F., Johansen, J. L., Johnson, D., Jokela, E. J., Joly, C. A., Jordan, G. J., Joseph, G. S., Junaedi, D., Junker, R. R., Justes, E., Kabzems, R., Kane, J., Kaplan, Z., Kattenborn, T., Kavelenova, L., Kearsley, E., Kempel, A., Kenzo, T., Kerkhoff, A., Khalil, M. I., Kinlock, N. L., Kissling, W. D., Kitajima, K., Kitzberger, T., Kjøller, R., Klein, T., Kleyer, M., Klimešová, J., Klipel, J., Kloeppel, B., Klotz, S., Knops, J. M., Kohyama, T., Koike, F., Kollmann, J., Komac, B., Komatsu, K., König, C., Kraft, N. J., Kramer, K., Kreft, H., Kühn, I., Kumarathunge, D., Kuppler, J., Kurokawa, H., Kurosawa, Y., Kuyah, S., Laclau, J. P., Lafleur, B., Lallai, E., Lamb, E., Lamprecht, A., Larkin, D. J., Laughlin, D., Le Bagousse-Pinguet, Y., le Maire, G., le Roux, P. C., le Roux, E., Lee, T., Lens, F., Lewis, S. L., Lhotsky, B., Li, Y., Li, X., Lichstein, J. W., Liebergesell, M., Lim, J. Y., Lin, Y. S., Linares, J. C., Liu, C., Liu, D., Liu, U., Livingstone, S., Llusià, J., Lohbeck, M., López-García, Á., Lopez-Gonzalez, G., Lososová, Z., Louault, F., Lukács, B. A., Lukeš, P., Luo, Y., Lussu, M., Ma, S., Maciel Rabelo Pereira, C., Mack, M., Maire, V., Mäkelä, A., Mäkinen, H., Malhado, A. C. M., Mallik, A., Manning, P., Manzoni, S., Marchetti, Z., Marchino, L., Marcilio-Silva, V., Marcon, E., Marignani, M., Markesteijn, L., Martin, A., Martínez-Garza, C., Martínez-Vilalta, J., Mašková, T., Mason, K., Mason, N., Massad, T. J., Masse, J., Mayrose, I., McCarthy, J., McCormack, M. L., McCulloh, K., McFadden, I. R., McGill, B. J., McPartland, M. Y., Medeiros, J. S., Medlyn, B., Meerts, P., Mehrabi, Z., Meir, P., Melo, F. P., Mencuccini, M., Meredieu, C., Messier, J., Mészáros, I., Metsaranta, J., Michaletz, S. T., Michelaki, C., Migalina, S., Milla, R.,

Miller, J. E., Minden, V., Ming, R., Mokany, K., Moles, A. T., Molnár, A., Molofsky, J., Molz, M., Montgomery, R. A., Monty, A., Moravcová, L., Moreno-Martínez, A., Moretti, M., Mori, A. S., Mori, S., Morris, D., Morrison, J., Mucina, L., Mueller, S., Muir, C. D., Müller, S. C., Munoz, F., Myers-Smith, I. H., Myster, R. W., Nagano, M., Naidu, S., Narayanan, A., Natesan, B., Negoita, L., Nelson, A. S., Neuschulz, E. L., Ni, J., Niedrist, G., Nieto, J., Niinemets, Ü., Nolan, R., Nottebrock, H., Nouvellon, Y., Novakovskiy, A., Nystuen, K. O., O'Grady, A., O'Hara, K., O'Reilly-Nugent, A., Oakley, S., Oberhuber, W., Ohtsuka, T., Oliveira, R., Öllerer, K., Olson, M. E., Onipchenko, V., Onoda, Y., Onstein, R. E., Ordonez, J. C., Osada, N., Ostonen, I., Ottaviani, G., Otto, S., Overbeck, G. E., Ozinga, W. A., Pahl, A. T., Paine, C. E., Pakeman, R. J., Papageorgiou, A. C., Parfionova, E., Pärtel, M., Patacca, M., Paula, S., Paule, J., Pauli, H., Pausas, J. G., Peco, B., Penuelas, J., Perea, A., Peri, P. L., Petisco-Souza, A. C., Petraglia, A., Petritan, A. M., Phillips, O. L., Pierce, S., Pillar, V. D., Pisek, J., Pomogaybin, A., Poorter, H., Portsmuth, A., Poschlod, P., Potvin, C., Pounds, D., Powell, A. S., Power, S. A., Prinzing, A., Puglielli, G., Pyšek, P., Raevel, V., Rammig, A., Ransijn, J., Ray, C. A., Reich, P. B., Reichstein, M., Reid, D. E., Réjou-Méchain, M., de Dios, V. R., Ribeiro, S., Richardson, S., Riibak, K., Rillig, M. C., Riviera, F., Robert, E. M., Roberts, S., Robroek, B., Roddy, A., Rodrigues, A. V., Rogers, A., Rollinson, E., Rolo, V., Römermann, C., Ronzhina, D., Roscher, C., Rosell, J. A., Rosenfield, M. F., Rossi, C., Roy, D. B., Royer-Tardif, S., Rüger, N., Ruiz-Peinado, R., Rumpf, S. B., Rusch, G. M., Ryo, M., Sack, L., Saldaña, A., Salgado-Negret, B., Salguero-Gomez, R., Santa-Regina, I., Santacruz-García, A. C., Santos, J., Sardans, J., Schamp, B., Scherer-Lorenzen, M., Schleuning, M., Schmid, B., Schmidt, M., Schmitt, S., Schneider, J. V., Schowanek, S. D., Schrader, J., Schrodt, F., Schuldt, B., Schurr, F., Selaya Garvizu, G., Semchenko, M., Seymour, C., Sfair, J. C., Sharpe, J. M., Sheppard, C. S., Sheremetiev, S., Shiodera, S., Shipley, B., Shovon, T. A., Siebenkäs, A., Sierra, C., Silva, V., Silva, M., Sitzia, T., Sjöman, H., Slot, M., Smith, N. G., Sodhi, D., Soltis, P., Soltis, D., Somers, B., Sonnier, G., Sørensen, M. V., Sosinski, E. E., Soudzilovskaia, N. A., Souza, A. F., Spasojevic, M., Sperandii, M. G., Stan, A. B., Stegen, J., Steinbauer, K., Stephan, J. G., Sterck, F., Stojanovic, D. B., Strydom, T., Suarez, M. L., Svenning, J. C., Svitková, I., Svitok, M., Svoboda, M., Swaine, E., Swenson, N., Tabarelli, M., Takagi, K., Tappeiner, U., Tarifa, R., Tauugourdeau, S., Tavsanoglu, C., te Beest, M., Tedersoo, L., Thiffault, N., Thom, D., Thomas, E., Thompson, K., Thornton, P. E., Thuiller, W., Tichý, L., Tissue, D., Tjoelker, M. G., Tng, D. Y. P., Tobias, J., Török, P., Tarin, T., Torres-Ruiz, J. M., Tóthmérész, B., Treurnicht, M., Trivellone, V., Trolliet, F., Trotsiuk, V., Tsakalos, J. L., Tsiripidis, I., Tysklind, N., Umehara, T., Usoltsev, V., Vadeboncoeur, M., Vaezi, J., Valladares, F., Vamosi, J., van Bodegom, P. M., van Breugel, M., Van Cleemput, E., van de Weg, M., van der Merwe, S., van der Plas, F., van der Sande, M. T., van Kleunen, M., Van Meerbeek, K., Vanderwel, M., Vanselow, K. A., Vårhammar, A., Varone, L., Vasquez Valderrama, M. Y., Vassilev, K., Vellend, M., Veneklaas, E. J., Verbeeck, H., Verheyen, K., Vibrans, A., Vieira, I., Villacís, J., Violle, C., Vivek, P., Wagner, K., Waldram, M., Waldron, A., Walker, A. P., Waller, M., Walther, G., Wang, H., Wang, F., Wang, W., Watkins, H., Watkins, J., Weber, U., Weedon, J. T., Wei, L., Weigelt, P., Weiher, E., Wells, A. W., Wellstein, C., Wenk, E., Westoby, M., Westwood, A., White, P. J., Whitten, M., Williams, M., Winkler, D. E., Winter, K., Womack, C., Wright, I. J., Wright, S. J., Wright, J., Pinho, B. X., Ximenes, F., Yamada, T., Yamaji, K., Yanai, R., Yankov, N., Yguel, B., Zanini, K. J., Zanne, A. E., Zelený, D., Zhao, Y. P., Zheng, J., Zheng, J., Ziemińska, K., Zirbel, C. R., Zizka, G., Zo-Bi, I. C., Zotz, G., and Wirth, C.: TRY plant trait database – enhanced coverage and open access, Global Change Biology, 26, 119–188, https://doi.org/10.1111/gcb.14904, 2020.

Keenan, T., Sabate, S., and Gracia, C.: The importance of mesophyll conductance in regulating forest ecosystem productivity during drought periods, Global Change Biology, 16, 1019–1034, https://doi.org/10.1111/j.1365-2486.2009.02017.x, 2010.

Kling, H., Fuchs, M., and Paulin, M.: Runoff conditions in the upper Danube basin under an ensemble of climate change scenarios, Journal of Hydrology, 424-425, 264–277, https://doi.org/10.1016/j.jhydrol.2012.01.011, http://dx.doi.org/10.1016/j.jhydrol.2012.01.011, 2012.

Knox, S. H., Sturtevant, C., Matthes, J. H., Koteen, L., Verfaillie, J., and Baldocchi, D.: Agricultural peatland restoration: Effects of land-use change on greenhouse gas (CO2 and CH4) fluxes in the Sacramento-San Joaquin Delta, Global Change Biology, 21, 750–765, https://doi.org/10.1111/gcb.12745, 2015.

Koebsch, F., Sonnentag, O., Järveoja, J., Peltoniemi, M., Alekseychik, P., Aurela, M., Arslan, A. N., Dinsmore, K., Gianelle, D., Helfter, C., Jackowicz-Korczynski, M., Korrensalo, A., Leith, F., Linkosalmi, M., Lohila, A., Lund, M., Maddison, M., Mammarella, I., Mander, Ü., Minkkinen, K., Pickard, A., Pullens, J. W., Tuittila, E. S., Nilsson, M. B., and Peichl, M.: Refining the role of phenology in regulating gross ecosystem productivity across European peatlands, Global Change Biology, 26, 876–887, https://doi.org/10.1111/gcb.14905, 2020.

Krinner, G., Viovy, N., de Noblet-Ducoudré, N., Ogée, J., Polcher, J., Friedlingstein, P., Ciais, P., Sitch, S., and Prentice, I. C.: A dynamic global vegetation model for studies of the coupled atmosphere-biosphere system, Global Biogeochemical Cycles, 19, 1–33, https://doi.org/10.1029/2003GB002199, http://doi.wiley.com/10.1029/2003GB002199, 2005.

Lafleur, P. M., Roulet, N. T., Bubier, J. L., Frolking, S., and Moore, T. R.: Interannual variability in the peatland-atmosphere carbon dioxide exchange at an ombrotrophic bog, Global Biogeochemical Cycles, 17, 1–14, https://doi.org/10.1029/2002gb001983, 2003.

Laine, A. M., Korrensalo, A., and Tuittila, E. S.: Plant functional traits play the second fiddle to plant functional types in explaining peatland CO2 and CH4 gas exchange, Science of the Total Environment, 834, 155 352, https://doi.org/10.1016/j.scitotenv.2022.155352, https://doi.org/10.1016/j.scitotenv.2022.155352, 2022.

Li, T., Raivonen, M., Alekseychik, P., Aurela, M., Lohila, A., Zheng, X., Zhang, Q., Wang, G., Mammarella, I., Rinne, J., Yu, L., Xie, B., Vesala, T., and Zhang, W.: Importance of vegetation classes in modeling CH4 emissions from boreal and subarctic wetlands in Finland, Science of the Total Environment, 572, 1111–1122, https://doi.org/10.1016/j.scitotenv.2016.08.020, http://dx.doi.org/10.1016/j.scitotenv.2016.08.020, 2016.

Lippmann, T. J., Zandt, M. H., Van Der Putten, N. N., Busschers, F. S., Hijma, M. P., Van Der Velden, P., De Groot, T., Van Aalderen, Z., Meisel, O. H., Slomp, C. P., Niemann, H., Jetten, M. S., Dolman, H. A., and Welte, C. U.: Microbial activity, methane production, and carbon storage in Early Holocene North Sea peats, Biogeosciences, 18, 5491–5511, https://doi.org/10.5194/bg-18-5491-2021, 2021.

Lippmann, T. J. R. and van Huissteden, J.: Peatland-VU-NUCOM (PVN 1.0): A peatland GHG emissions model using dynamic plant functional types, https://doi.org/https://doi.org/10.5281/zenodo.7701698, https://zenodo.org/record/7701698, 2023.

Littleton, E. W., Harper, A. B., Vaughan, N. E., Oliver, R. J., Duran-Rojas, M. C., and Lenton, T. M.: JULES-BE: Representation of bioenergy crops and harvesting in the Joint UK Land Environment Simulator vn5.1, Geoscientific Model Development, 13, 1123–1136, https://doi.org/10.5194/gmd-13-1123-2020, https://gmd.copernicus.org/articles/13/1123/2020/, 2020.

Loisel, J., Gallego-Sala, A. V., Amesbury, M. J., Magnan, G., Anshari, G., Beilman, D. W., Benavides, J. C., Blewett, J., Camill, P., Charman, D. J., Chawchai, S., Hedgpeth, A., Kleinen, T., Korhola, A., Large, D., Mansilla, C. A., Müller, J., van Bellen, S., West, J. B., Yu, Z., Bubier, J. L., Garneau, M., Moore, T., Sannel, A. B., Page, S., Väliranta, M., Bechtold, M., Brovkin, V., Cole, L. E., Chanton, J. P., Christensen, T. R., Davies, M. A., De Vleeschouwer, F., Finkelstein, S. A., Frolking, S., Gałka, M., Gandois, L., Girkin, N., Harris, L. I., Heinemeyer, A., Hoyt, A. M., Jones, M. C., Joos, F., Juutinen, S., Kaiser, K., Lacourse, T., Lamentowicz, M., Larmola, T., Leifeld, J., Lohila, A., Milner, A. M., Minkkinen, K., Moss, P., Naafs, B. D., Nichols, J., O'Donnell, J., Payne, R., Philben, M., Piilo, S., Quillet, A., Ratnayake, A. S., Roland, T. P., Sjögersten, S., Sonnentag, O., Swindles, G. T., Swinnen, W., Talbot, J., Treat, C., Valach, A. C., and Wu, J.: Expert assessment of future vulnerability of the global peatland carbon sink, Nature Climate Change, 11, 70–77, https://doi.org/10.1038/s41558-020-00944-0, 2021.

Malmer, N., Albinsson, C., Svensson, B. M., and Wallén, B.: Interferences between Sphagnum and vascular plants: Effects on plant community structure and peat formation, Oikos, 100, 469–482, https://doi.org/10.1034/j.1600-0706.2003.12170.x, 2003.

Malmer, N., Johansson, T., Olsrud, M., and Christensen, T. R.: Vegetation, climatic changes and net carbon sequestration in a North-Scandinavian subarctic mire over 30 years, Global Change Biology, 11, 1895–1909, https://doi.org/10.1111/j.1365-2486.2005.01042.x, 2005.

Masson-Delmotte, V., Zhai, P., Pirani, A., Connors, S. L., Péan, C., Berger, S., Caud, N., Chen, Y., Goldfarb, L., Gomis, M. I., Huang, M., Leitzell, K., Lonnoy, E., Matthews, J. B. R., Maycock, T. K., Waterfield, T., Yelekçi, O., Yu, R., and Zhou, B., eds.: Climate Change 2021: The Physical Science Basis. Contribution of Working Group I to the Sixth Assessment Report of the Intergovernmental Panel on Climate Change, vol. In Press, Cambridge University Press, Cambridge, United Kingdom and New York, NY, USA, https://doi.org/10.1017/9781009157896, 2021.

Mazzola, V., Perks, M. P., Smith, J., Yeluripati, J., and Xenakis, G.: Assessing soil carbon dioxide and methane fluxes from a Scots pine raised bog-edge-woodland, Journal of Environmental Management, 302, 114 061, https://doi.org/10.1016/j.jenvman.2021.114061, https://doi.org/10.1016/j.jenvman.2021.114061, 2022.

Melillo, J. M., Steudler, P. A., Aber, J. D., Newkirk, K., Lux, H., Bowles, F. P., Catricala, C., Magill, A., Ahrens, T., and Morrisseau, S.: Soil warming and carbon-cycle feedbacks to the climate system, Science, 298, 2173–2176, https://doi.org/10.1126/science.1074153, 2002.

Melton, J. R., Wania, R., Hodson, E. L., Poulter, B., Ringeval, B., Spahni, R., Bohn, T., Avis, C. A., Beerling, D. J., Chen, G., Eliseev, A. V., Denisov, S. N., Hopcroft, P. O., Lettenmaier, D. P., Riley, W. J., Singarayer, J. S., Subin, Z. M., Tian, H., Zürcher, S., Brovkin, V., van Bodegom, P. M., Kleinen, T., Yu, Z. C., and Kaplan, J. O.: Present state of global wetland extent and wetland methane modelling: conclusions from a model inter-comparison project (WETCHIMP), Biogeosciences, 10, 753–788, https://doi.org/10.5194/bg-10-753-2013, https://bg.copernicus.org/articles/10/753/2013/, 2013.

Metzger, C., Jansson, P. E., Lohila, A., Aurela, M., Eickenscheidt, T., Belelli-Marchesini, L., Dinsmore, K. J., Drewer, J., Van Huissteden, J., and Drösler, M.: CO2 fluxes and ecosystem dynamics at five European treeless peatlands-merging data and process oriented modeling, Biogeosciences, 12, 125–146, https://doi.org/10.5194/bg-12-125-2015, http://www.biogeosciences.net/12/125/2015/https://bg.copernicus.org/articles/12/125/2015/, 2015.

Mi, Y., Van Huissteden, J., Parmentier, F. J. W., Gallagher, A., Budishchev, A., Berridge, C. T., and Dolman, A. J.: Improving a plot-scale methane emission model and its performance at a northeastern Siberian tundra site, Biogeosciences, 11, 3985–3999, https://doi.org/10.5194/bg-11-3985-2014, 2014.

Moore, T. R., Bubier, J. L., and Bledzki, L.: Litter decomposition in temperate peatland ecosystems: The effect of substrate and site, Ecosystems, 10, 949–963, https://doi.org/10.1007/s10021-007-9064-5, http://link.springer.com/10.1007/s10021-007-9064-5, 2007.

Morin, T. H., Bohrer, G., Frasson, R. P., Naor-Azreli, L., Mesi, S., Stefanik, K. C., and Schäfer, K. V.: Environmental drivers of methane fluxes from an urban temperate wetland park, Journal of Geophysical Research: Biogeosciences, 119, 2188–2208, https://doi.org/10.1002/2014JG002750, 2014a.

Morin, T. H., Bohrer, G., Naor-Azrieli, L., Mesi, S., Kenny, W. T., Mitsch, W. J., and Schäfer, K. V. R.: The seasonal and diurnal dynamics of methane flux at a created urban wetland, Ecological Engineering, 72, 74–83, https://doi.org/10.1016/j.ecoleng.2014.02.002, http://dx.doi.org/10.1016/j.ecoleng.2014.02.002, 2014b.

Morin, T. H., Bohrer, G., Stefanik, K. C., Rey-Sanchez, A. C., Matheny, A. M., and Mitsch, W. J.: Combining eddy-covariance and chamber measurements to determine the methane budget from a small, heterogeneous urban floodplain wetland park, Agricultural and Forest Meteorology, 237-238, 160–170, https://doi.org/10.1016/j.agrformet.2017.01.022, http://dx.doi.org/10.1016/j.agrformet.2017.01.022, 2017.

Muñoz-Sabater, J., Dutra, E., Agustí-Panareda, A., Albergel, C., Arduini, G., Balsamo, G., Boussetta, S., Choulga, M., Harrigan, S., Hersbach, H., Martens, B., Miralles, D. G., Piles, M., Rodríguez-Fernández, N. J., Zsoter, E., Buontempo, C., and Thépaut, J. N.: ERA5-Land:

A state-of-the-art global reanalysis dataset for land applications, Earth System Science Data, 13, 4349–4383, https://doi.org/10.5194/essd-13-4349-2021, 2021.

Ostle, N. J., Smith, P., Fisher, R., Ian Woodward, F., Fisher, J. B., Smith, J. U., Galbraith, D., Levy, P., Meir, P., McNamara, N. P., and Bardgett, R. D.: Integrating plant-soil interactions into global carbon cycle models, Journal of Ecology, 97, 851–863, https://doi.org/10.1111/j.1365-2745.2009.01547.x, 2009.

Pangala, S. R., Moore, S., Hornibrook, E. R., and Gauci, V.: Trees are major conduits for methane egress from tropical forested wetlands, New Phytologist, 197, 524–531, https://doi.org/10.1111/nph.12031, 2013.

Pavelka, M., Acosta, M., Kiese, R., Altimir, N., Brümmer, C., Crill, P., Darenova, E., Fuß, R., Gielen, B., Graf, A., Klemedtsson, L., Lohila, A., Longdoz, B., Lindroth, A., Nilsson, M., Jiménez, S. M., Merbold, L., Montagnani, L., Peichl, M., Pihlatie, M., Pumpanen, J., Ortiz, P. S., Silvennoinen, H., Skiba, U., Vestin, P., Weslien, P., Janous, D., and Kutsch, W.: Standardisation of chamber technique for CO 2 , N 2 O and CH 4 fluxes measurements from terrestrial ecosystems, International Agrophysics, 32, 569–587, https://doi.org/10.1515/intag-2017-0045, 2018.

Peltoniemi, K., Fritze, H., and Laiho, R.: Response of fungal and actinobacterial communities to water-level drawdown in boreal peatland sites, Soil Biology and Biochemistry, 41, 1902–1914, https://doi.org/10.1016/j.soilbio.2009.06.018, http://dx.doi.org/10.1016/j.soilbio.2009.06.018, 2009.

Puma, M. J., Koster, R. D., and Cook, B. I.: Phenological versus meteorological controls on land-atmosphere water and carbon fluxes, Journal of Geophysical Research: Biogeosciences, 118, 14–29, https://doi.org/10.1029/2012JG002088, 2013.

Saarnio, S., Wittenmayer, L., and Merbach, W.: Rhizospheric exudation of Eriophorum vaginatum L. — Potential link to methanogenesis, Plant and Soil, 267, 343–355, https://doi.org/10.1007/s11104-005-0140-3, 2004.

Saleska, S. R., Shaw, M. R., Fischer, M. L., Dunne, J. A., Still, C. J., Holman, M. L., and Harte, J.: Plant community composition mediates both large transient decline and predicted long-term recovery of soil carbon under climate warming, Global Biogeochemical Cycles, 16, 3–1–3–18, https://doi.org/10.1029/2001gb001573, 2002.

Saunois, M., R. Stavert, A., Poulter, B., Bousquet, P., G. Canadell, J., B. Jackson, R., A. Raymond, P., J. Dlugokencky, E., Houweling, S., K. Patra, P., Ciais, P., K. Arora, V., Bastviken, D., Bergamaschi, P., R. Blake, D., Brailsford, G., Bruhwiler, L., M. Carlson, K., Carrol, M., Castaldi, S., Chandra, N., Crevoisier, C., M. Crill, P., Covey, K., L. Curry, C., Etiope, G., Frankenberg, C., Gedney, N., I. Hegglin, M., Höglund-Isaksson, L., Hugelius, G., Ishizawa, M., Ito, A., Janssens-Maenhout, G., M. Jensen, K., Joos, F., Kleinen, T., B. Krummel, P., L. Langenfelds, R., G. Laruelle, G., Liu, L., MacHida, T., Maksyutov, S., C. McDonald, K., McNorton, J., A. Miller, P., R. Melton, J., Morino, I., Müller, J., Murguia-Flores, F., Naik, V., Niwa, Y., Noce, S., O'Doherty, S., J. Parker, R., Peng, C., Peng, S., P. Peters, G., Prigent, C., Prinn, R., Ramonet, M., Regnier, P., J. Riley, W., A. Rosentreter, J., Segers, A., J. Simpson, I., Shi, H., J. Smith, S., Paul Steele, L., F. Thornton, B., Tian, H., Tohjima, Y., N. Tubiello, F., Tsuruta, A., Viovy, N., Voulgarakis, A., S. Weber, T., Van Weele, M., R. Van Der Werf, G., F. Weiss, R., Worthy, D., Wunch, D., Yin, Y., Yoshida, Y., Zhang, W., Zhang, Z., Zhao, Y., Zheng, B., Zhu, Q., Zhu, Q., and Zhuang, Q.: The global methane budget 2000-2017, Earth System Science Data, 12, 1561–1623, https://doi.org/10.5194/essd-12-1561-2020, 2020.

Schipper, L. A. and Reddy, K. R.: Determination of Methane Oxidation in the Rhizosphere of Sagittaria lancifolia Using Methyl Fluoride, Soil Science Society of America Journal, 60, 611–616, https://doi.org/10.2136/sssaj1996.03615995006000020039x, 1996.

Schrier-Uijl, A. P., Kroon, P. S., Hendriks, D. M. D., Hensen, A., Van Huissteden, J., Berendse, F., and Veenendaal, E. M.: Agricultural peatlands: Towards a greenhouse gas sink - A synthesis of a Dutch landscape study, Biogeosciences, 11, 4559–4576, https://doi.org/10.5194/bg-11-4559-2014, 2014.

Smith, B., Prentice, I. C., and Sykes, M. T.: Representation of vegetation dynamics in the modelling of terrestrial ecosystems: comparing two contrasting approaches within European climate space, Global Ecology and Biogeography, 10, 621–637, https://doi.org/10.1046/j.1466-822x.2001.t01-1-00256.x, 2001.

Smithwick, E. A., Lucash, M. S., McCormack, M. L., and Sivandran, G.: Improving the representation of roots in terrestrial models, Ecological Modelling, 291, 193–204, https://doi.org/10.1016/j.ecolmodel.2014.07.023, http://dx.doi.org/10.1016/j.ecolmodel.2014.07.023, 2014.

Spahni, R., Wania, R., Neef, L., Van Weele, M., Pison, I., Bousquet, P., Frankenberg, C., Foster, P. N., Joos, F., Prentice, I. C., and Van Velthoven, P.: Constraining global methane emissions and uptake by ecosystems, Biogeosciences, 8, 1643–1665, https://doi.org/10.5194/bg-8-1643-2011, 2011.

Speckman, H. N., Frank, J. M., Bradford, J. B., Miles, B. L., Massman, W. J., Parton, W. J., and Ryan, M. G.: Forest ecosystem respiration estimated from eddy covariance and chamber measurements under high turbulence and substantial tree mortality from bark beetles, Global Change Biology, 21, 708–721, https://doi.org/10.1111/gcb.12731, 2015.

Strack, M., Waller, M. F., and Waddington, J. M.: Sedge succession and peatland methane dynamics: A potential feedback to climate change, Ecosystems, 9, 278–287, https://doi.org/10.1007/s10021-005-0070-1, 2006.

Ström, L., Mastepanov, M., and Christensen, T. R.: Species-specific Effects of Vascular Plants on Carbon Turnover and Methane Emissions from Wetlands, Biogeochemistry, 75, 65–82, https://doi.org/10.1007/s10533-004-6124-1, https://doi.org/10.1007/s10533-004-6124-1http://link.springer.com/10.1007/s10533-004-6124-1, 2005.

Ström, L., Falk, J. M., Skov, K., Jackowicz-Korczynski, M., Mastepanov, M., Christensen, T. R., Lund, M., and Schmidt, N. M.: Controls of spatial and temporal variability in CH4 flux in a high arctic fen over three years, Biogeochemistry, 125, 21–35, https://doi.org/10.1007/s10533-015-0109-0, 2015.

Tiemeyer, B., Albiac Borraz, E., Augustin, J., Bechtold, M., Beetz, S., Beyer, C., Drosler, M., Ebli, M., Eickenscheidt, T., Fiedler, S., Forster, C., Freibauer, A., Giebels, M., Glatzel, S., Heinichen, J., Hoffmann, M., Hoper, H., Jurasinski, G., Leiber-Sauheitl, K., Peichl-Brak, M., Rosskopf, N., Sommer, M., and Zeitz, J.: High emissions of greenhouse gases from grasslands on peat and other organic soils, Global Change Biology, 22, 4134–4149, https://doi.org/10.1111/gcb.13303, 2016.

Toet, S., Cornelissen, J. H., Aerts, R., Van Logtestijn, R. S., De Beus, M., and Stoevelaar, R.: Moss responses to elevated CO2 and variation in hydrology in a temperate lowland peatland, Plant Ecology, 182, 27–40, https://doi.org/10.1007/s11258-005-9029-8, 2006.

Tramontana, G., Jung, M., Schwalm, C. R., Ichii, K., Camps-Valls, G., Ráduly, B., Reichstein, M., Arain, M. A., Cescatti, A., Kiely, G., Merbold, L., Serrano-Ortiz, P., Sickert, S., Wolf, S., and Papale, D.: Predicting carbon dioxide and energy fluxes across global FLUXNET sites with regression algorithms, Biogeosciences, 13, 4291–4313, https://doi.org/10.5194/bg-13-4291-2016, 2016.

Van den Hoof, C., Hanert, E., and Vidale, P. L.: Simulating dynamic crop growth with an adapted land surface model - JULES-SUCROS: Model development and validation, Agricultural and Forest Meteorology, 151, 137–153, https://doi.org/10.1016/j.agrformet.2010.09.011, https://linkinghub.elsevier.com/retrieve/pii/S0168192310002571, 2011.

van Geel, B., Bos, J. M., and Pals, J. P.: Archaeological and palaeoecological aspects of a medieval house terp in a reclaimed raiseg bog area in North Holland, Ber. Rijksd. Oudheidkd. Bodemonderz, 33, 419–444, 1983.

van Huissteden, J., van den Bos, R., and Marticorena Alvarez, I.: Modelling the effect of water-table management on CO2 and CH4 fluxes from peat soils, Geologie en Mijnbouw/Netherlands Journal of Geosciences, 85, 3–18, https://doi.org/10.1017/S0016774600021399, 2006.

van Huissteden, J., Petrescu, a. M. R., Hendriks, D. M. D., and Rebel, K. T.: Sensitivity analysis of a wetland methane emission model based on temperate and Arctic wetland sites, Biogeosciences, 6, 9083–9126, https://doi.org/10.5194/bgd-6-9083-2009, 2009.

Waddington, J. M. and Roulet, N. T.: Carbon balance of a Boreal patterned peatland, Global Change Biology, 6, 87–97, https://doi.org/10.1046/j.1365-2486.2000.00283.x, 2000.

Walter, B. P. and Heimann, M.: A process-based, climate-sensitive model to derive methane emissions from natural wetlands: Application to five wetland sites, sensitivity to model parameters, and climate, Global Biogeochemical Cycles, 14, 745–765, https://doi.org/10.1029/1999GB001204, 2000.

Walter, B. P., Heimann, M., and Matthews, E.: Modeling modern methane emissions from natural wetlands 2. Interannual variations 1982-1993, Journal of Geophysical Research Atmospheres, 106, 34 207–34 219, https://doi.org/10.1029/2001JD900164, 2001.

Wania, R., Ross, I., and Prentice, I. C.: Implementation and evaluation of a new methane model within a dynamic global vegetation model: LPJ-WHyMe v1.3.1, Geoscientific Model Development, 3, 565–584, https://doi.org/10.5194/gmd-3-565-2010, 2010.

Wania, R., Melton, J. R., Hodson, E. L., Poulter, B., Ringeval, B., Spahni, R., Bohn, T., Avis, C. A., Chen, G., Eliseev, A. V., Hopcroft, P. O., Riley, W. J., Subin, Z. M., Tian, H., Van Bodegom, P. M., Kleinen, T., Yu, Z. C., Singarayer, J. S., Zürcher, S., Lettenmaier, D. P., Beerling, D. J., Denisov, S. N., Prigent, C., Papa, F., and Kaplan, J. O.: Present state of global wetland extent and wetland methane modelling: Methodology of a model inter-comparison project (WETCHIMP), Geoscientific Model Development, 6, 617–641, https://doi.org/10.5194/gmd-6-617-2013, 2013.

WGI, I. A.: Climate Change 2021 The Physical Science Basis WGI, vol. 34, 2021.

Whipps, J. M.: Carbon economy., The rhizosphere., pp. 59–97, 1990.

Wu, Y. and Blodau, C.: PEATBOG: a biogeochemical model for analyzing coupled carbon and nitrogen dynamics in northern peatlands, Geoscientific Model Development, 6, 1173–1207, https://doi.org/10.5194/gmd-6-1173-2013, https://gmd.copernicus.org/articles/6/1173/2013/, 2013.

Wu, Y., Verseghy, D. L., and Melton, J. R.: Integrating peatlands into the coupled Canadian Land Surface Scheme (CLASS) v3.6 and the Canadian Terrestrial Ecosystem Model (CTEM) v2.0, Geoscientific Model Development, 9, 2639–2663, https://doi.org/10.5194/gmd-9-2639-2016, https://gmd.copernicus.org/articles/9/2639/2016/, 2016.

Wullschleger, S. D., Epstein, H. E., Box, E. O., Euskirchen, E. S., Goswami, S., Iversen, C. M., Kattge, J., Norby, R. J., Van Bodegom, P. M., and Xu, X.: Plant functional types in Earth system models: Past experiences and future directions for application of dynamic vegetation models in high-latitude ecosystems, Annals of Botany, 114, 1–16, https://doi.org/10.1093/aob/mcu077, https://academic.oup.com/aob/article-lookup/doi/10.1093/aob/mcu077, 2014.

Yrjälä, K., Tuomivirta, T., Juottonen, H., Putkinen, A., Lappi, K., Tuittila, E. S., Penttilä, T., Minkkinen, K., Laine, J., Peltoniemi, K., and Fritze, H.: CH4 production and oxidation processes in a boreal fen ecosystem after long-term water table drawdown, Global Change Biology, 17, 1311–1320, https://doi.org/10.1111/j.1365-2486.2010.02290.x, 2011.

Yu, Z., Loisel, J., Brosseau, D. P., Beilman, D. W., and Hunt, S. J.: Global peatland dynamics since the Last Glacial Maximum, Geophysical Research Letters, 37, 1–5, https://doi.org/10.1029/2010GL043584, 2010.

Zeng, X.: Global Vegetation Root Distribution for Land Modeling, Journal of Hydrometeorology, 2, 525–530, https://doi.org/10.1175/1525-7541(2001)002<0525:gvrdfl>2.0.co;2, 2001.

Zhao, J., Lange, H., and Meissner, H.: Gap-filling continuously-measured soil respiration data: A highlight of time-series-based methods, Agricultural and Forest Meteorology, 285-286, 107 912, https://doi.org/10.1016/j.agrformet.2020.107912, https://doi.org/10.1016/j.agrformet.2020.107912, 2020.

Zuo, Z. Y. and Xiao, D.: Linking global to regional climate change, in: Climate Change Research, edited by Masson-Delmotte, V., Zhai, P., Pirani, A., Connors, S. L., Péan, C., Berger, S., Caud, N., Chen, Y., Goldfarb, L., Gomis, M. I., Huang, M., Leitzell, K., Lonnoy, E.,

Matthews, J. B. R., Maycock, T. K., Waterfield, T., Yelekçi, O., Yu, R., and Zhou, B., vol. 17, pp. 705–712, Cambridge University Press,
1460 Cambridge, United Kingdom and New York, NY, USA, https://doi.org/10.12006/j.issn.1673-1719.2021.176, https://www.ipcc.ch/, 2021.